Stationary Waves Weaken and Delay the Near-Surface Response to Stratospheric Ozone Depletion

CHAIM I. GARFINKEL,[a] IAN WHITE,[a] EDWIN P. GERBER,[b] SEOK-WOO SON,[c] AND MARTIN JUCKER[d]

[a] *The Hebrew University of Jerusalem, Institute of Earth Sciences, Edmond J. Safra Campus, Givat Ram, Jerusalem, Israel*
[b] *Courant Institute of Mathematical Sciences, New York University, New York*
[c] *School of Earth and Environmental Sciences, Seoul National University, Seoul, South Korea*
[d] *Climate Change Research Centre and ARC Centre of Excellence for Climate Extremes, University of New South Wales, Sydney, New South Wales, Australia*

(Manuscript received 10 November 2021, in final form 5 October 2022)

ABSTRACT: An intermediate-complexity moist general circulation model is used to investigate the factors controlling the magnitude of the surface impact from Southern Hemisphere springtime ozone depletion. In contrast to previous idealized studies, a model with full radiation is used; furthermore, the model can be run with a varied representation of the surface, from a zonally uniform aquaplanet to a configuration with realistic stationary waves. The model captures the observed summertime positive Southern Annular Mode response to stratospheric ozone depletion. While synoptic waves dominate the long-term poleward jet shift, the initial response includes changes in planetary waves that simultaneously moderate the polar cap cooling (i.e., a negative feedback) and also constitute nearly one-half of the initial momentum flux response that shifts the jet poleward. The net effect is that stationary waves weaken the circulation response to ozone depletion in both the stratosphere and troposphere and also delay the response until summer rather than spring when ozone depletion peaks. It is also found that Antarctic surface cooling in response to ozone depletion helps to strengthen the poleward shift; however, shortwave surface effects of ozone are not critical. These surface temperature and stationary wave feedbacks are strong enough to overwhelm the previously recognized jet latitude/persistence feedback, potentially explaining why some recent comprehensive models do not exhibit a clear relationship between jet latitude/persistence and the magnitude of the response to ozone. The jet response is shown to be linear with respect to the magnitude of the imposed stratospheric perturbation, demonstrating the usefulness of interannual variability in ozone depletion for subseasonal forecasting.

KEYWORDS: Antarctic Oscillation; Stationary waves; Stratosphere–troposphere coupling; Ozone; Shortwave radiation

1. Introduction

Antarctic springtime ozone concentrations in the lower stratosphere decreased in the last few decades of the twentieth century due to anthropogenic emissions of chlorofluorocarbons (Solomon et al. 1986), and only recently have begun the slow process of recovery (Weber et al. 2018). Ozone depletion is known to have been the dominant contributor over the late twentieth century to a poleward shift of the austral summer Southern Hemisphere (SH) tropospheric midlatitude jet and associated storm track and precipitation, often quantified by a positive index of the Southern Annular Mode (SAM), and to have led to an expansion of the summer Hadley cell (Trenberth and Stepaniak 2002; Gillett and Thompson 2003; Son et al. 2010; Thompson et al. 2011; Kang et al. 2011; Polvani et al. 2011b; McLandress et al. 2011; Eyring et al. 2013; Gerber and Son 2014; Gonzalez et al. 2014; Previdi and Polvani 2014; Waugh et al. 2015; Seviour et al. 2017; Son et al. 2018). Over the next ~50 years, ozone recovery is expected to nearly cancel out changes in the tropospheric jet and Hadley cell that would otherwise be forced by greenhouse gases (Son et al. 2008; Polvani et al. 2011a; Arblaster et al. 2011; Barnes and Polvani 2013; Gerber and Son 2014; Banerjee et al. 2020). Despite its importance, the mechanism whereby ozone depletion leads to a downward impact, and the details of how this mechanism governs the magnitude of the impact, are still unclear, as noted for example in successive WMO Ozone assessments (World Meteorological Organization 2011, 2014; Karpechko et al. 2018).

This study focuses on the role of stationary versus transient waves for the downward impact. While SH stationary waves are weaker than their counterparts in the Northern Hemisphere, they contribute roughly one-half of the heat flux in spring in the lower stratosphere (Kållberg et al. 2005) and contribute to the intermodel spread in the timing of the ozone-hole breakup (Hurwitz et al. 2010). A commonly used model in studies focusing on the mechanism(s) for the surface response to ozone depletion is a dry dynamical core with a flat bottom (e.g., Kushner and Polvani 2004; Sun et al. 2014; Yang et al. 2015; Smith and Scott 2016), allowing for transient planetary waves only, or a highly idealized mountain (Gerber and Polvani 2009; Domeisen et al. 2013). The importance of stationary waves in the SH for a surface response cannot be readily evaluated in such setups by construction. Many of

Supplemental information related to this paper is available at the Journals Online website: https://doi.org/10.1175/JCLI-D-21-0874.s1.

Corresponding author: Chaim I. Garfinkel, chaim.garfinkel@mail.huji.ac.il

DOI: 10.1175/JCLI-D-21-0874.1

these studies using flat-bottomed models nevertheless conclude that planetary waves are crucial for the surface response. For example, Smith and Scott (2016) find that the response to a stratospheric perturbation is weaker if interactions between planetary- and synoptic-scale waves are suppressed, while Domeisen et al. (2013) find that the jet shifts in the opposite direction if only planetary waves are present, ruling out the possibility that the jet shift occurs purely as a response to changes in the planetary- or synoptic-scale wave fields alone. However, the lack of stationary planetary waves in these models resembling those in the SH may lead to a misrepresentation of the total impact of planetary waves. The goal of this study is to answer this question: What is the relative role of synoptic versus planetary waves for the downward impact resulting from ozone depletion?

A secondary goal of this study is to disentangle the role of the surface temperature cooling in response to ozone depletion for the jet response. The SAM response appears to account for around half of the observed surface warming over the Antarctic Peninsula, nearly all of the observed cooling over East Antarctica, and much of the warming over Patagonia (Trenberth and Stepaniak 2002; Previdi and Polvani 2014). Nevertheless, radiative effects may also be important for the tropospheric (Grise et al. 2009) and the surface temperature (Yang et al. 2014) responses to ozone depletion, although Chiodo et al. (2017) found the net radiative effect at the surface to be weak. Regardless of how the tropospheric cooling arises, the role of this tropospheric cooling for the jet shift, as compared with other mechanisms for the downward impact, has not been isolated in previous work.

We take advantage of a recently developed intermediate-complexity model that can delineate the role of different wave types and of surface cooling. Namely, it can be run alternately with realistic stationary waves or without any zonal asymmetry in the bottom boundary (e.g., topography) and thus can clarify the role of stationary waves for the surface response. This model also allows us to carefully isolate the importance of surface temperature changes in response to ozone depletion by studying the jet response for different surface albedos over Antarctica.

After introducing this model in section 2 and our diagnostics in section 3, we demonstrate in section 4 that the model in its most realistic configuration simulates a quantitatively realistic response to ozone depletion, but that the response is significantly stronger in an aquaplanet configuration. We consider reasons for this effect in section 5, isolate the role of surface cooling in section 6, and then summarize our results and place them in the context of previous work in section 7.

2. An intermediate-complexity atmospheric model

We use the Model of an Idealized Moist Atmosphere (MiMA) introduced by Jucker and Gerber (2017), Garfinkel et al. (2020a,b). This model builds on the aquaplanet models of Frierson et al. (2006, 2007), and Merlis et al. (2013). Very briefly, the model solves the moist primitive equations on the sphere, employing a simplified Betts–Miller convection scheme (Betts 1986; Betts and Miller 1986), idealized boundary layer scheme based on Monin–Obukhov similarity theory, and a purely thermodynamic (or slab) ocean. An important feature for this paper is that we use a realistic radiation scheme—the Rapid Radiative Transfer Model (RRTMG; Mlawer et al. 1997; Iacono et al. 2000)—which allows us to explicitly simulate the radiative response to ozone depletion, unlike previous studies using more idealized models with Newtonian cooling. See Jucker and Gerber (2017) for more details.

This model can be run alternately as an aquaplanet, or with stationary waves quantitatively similar to those in comprehensive models (Garfinkel et al. 2020a,b). The most realistic configuration of MiMA used in this study has boundary forcings that are identical to those of Garfinkel et al. (2020a), and this configuration is referred to as STAT in the rest of this paper. MiMA has no true land; rather, the properties of the surface at grid points that are land on Earth are modified to mimic land (Fig. 3 of Jucker and Gerber 2017). The net effect is that the STAT configuration includes three sources of zonal asymmetry in the lower boundary: orography, prescribed east–west ocean heat transport, and land–sea contrast (i.e., difference in heat capacity, surface friction, and moisture availability between "ocean" grid points and "land" grid points). The specifications of these forcings can be found in Garfinkel et al. (2020a). The same albedo value is applied to all wavelengths of incoming solar radiation.

We analyze the response to an identical ozone hole for four different tropospheric configurations: (i) the Southern Hemisphere (SH) of STAT, (ii) the Northern Hemisphere (NH) of STAT (STATNH), (iii) an aquaplanet with albedo of 0.27 globally (including over "Antarctica"), and (iv) an aquaplanet but in which the albedo over Antarctica is increased to 0.8 and elsewhere lowered to 0.23 [as in STAT; see Eq. (A3) of Garfinkel et al. 2020a] to help maintain a similar global mean and "Antarctic" temperature to STAT. We refer to these last two experiments as AQUA27 and AQUA80 in the rest of this paper. The AQUA runs have no stationary waves, but both aquaplanet integrations still include north–south ocean heat transport [Eq. (A4) of Garfinkel et al. 2020a]. The aquaplanet runs use a mixed-layer depth of 75 m everywhere (including Antarctica) and oceanic settings for surface roughness; in contrast, STAT has a larger surface roughness and mixed layer depth of 2.5 m over land (including Antarctica), and a varying mixed-layer depth for ocean grid points [see Eq. (A2) of Garfinkel et al. 2020a]. The NH STAT configuration is not meant to simulate a boreal winter ozone "hole" either as observed in 1997, 2011, or 2020 (Hurwitz et al. 2011; Manney et al. 2011; Rao and Garfinkel 2020; Lawrence et al. 2020; Rao and Garfinkel 2021) or as in a world-avoided scenario (Newman et al. 2009; Garcia et al. 2012). Rather, it explores how the exact same ozone perturbation impacts the circulation with a very different climatology of stationary (and synoptic) waves.

For all tropospheric configurations, we compare a pair of simulations: 1) a preindustrial simulation forced with the monthly varying zonally averaged climatology of ozone in the CMIP6 ozone specification averaged from 1860 to 1899 (PI simulation; Checa-Garcia et al. 2018; Checa-Garcia 2018) and 2) a simulation forced with the monthly varying zonally averaged climatology of ozone in the CMIP6 ozone specification averaged from 1990 to 1999, which we then

further reduce by a factor of 4 over the pole between 150 and 30 hPa by multiplying by the factor $\Phi(\varphi)$:

$$\Phi(\varphi) = 1 - (3/8)\left[1 - \tanh\left(\frac{\varphi + 65^\circ}{3^\circ}\right)\right], \quad (1)$$

where φ denotes latitude. This additional reduction in the polar lower stratosphere is intended to capture springs with stronger-than-average ozone depletion (Previdi and Polvani 2014) and is included to enhance the signal-to-noise ratio. An experiment without this additional reduction leads to a weaker surface response, which is consistent with previous work that has argued that interannual variability of ozone concentrations can be used to improve the skill of seasonal and subseasonal forecasting (Son et al. 2013; Bandoro et al. 2014; Hendon et al. 2020; Jucker and Goyal 2022; Oh et al. 2022). The linearity of the response is discussed in more detail in section 5c. For the NH ozone-hole experiments, Eq. (1) is suitably modified to

$$\Phi(\varphi) = 1 - (3/8)\left[1 + \tanh\left(\frac{\varphi - 65^\circ}{3^\circ}\right)\right]$$

to place the additional reduction over the North Pole.

The ozone-hole runs branch from 1 October (1 March for STATNH) of each of the last 65 years of the respective preindustrial control runs for a total of 65 ensemble members, and these are then integrated for at least 150 days. The results are shown in terms of the difference between the ozone-hole simulation and the PI simulation (ozone hole − PI), although all conclusions are just as applicable to ozone recovery (with reversed sign). The net change of ozone is shown in Figs. 1a–c, which shows days 1–30 (October), 31–70 (November and early December), and 71–120 (the rest of December and January). The ozone perturbation is evident throughout the spring and decays in early summer. In the polar lower stratosphere, more than 90% of the preindustrial ozone is locally depleted, and this reduction is within the range of realistic values (Solomon et al. 2005; Previdi and Polvani 2014). Ozone actually increases slightly in the upper stratosphere in summer due to dynamical feedbacks (Stolarski et al. 2006). While differences in ozone at other latitudes and pressure levels are present, they are small and will be ignored in the rest of this work.

To isolate any effect of ozone on surface shortwave absorption (Grise et al. 2009; Yang et al. 2014; Chiodo et al. 2017), and also to more cleanly connect our results to studies using dry models with an imposed diabatic cooling (Kushner and Polvani 2004; Sheshadri and Plumb 2016), we also performed simulations in which a diabatic cooling perturbation is imposed in the lower stratosphere. Our goal is to match the stratospheric diabatic cooling perturbation due to ozone, and thus we show in Figs. 1d–f the net diabatic cooling perturbation as computed by the model in the presence of reduced ozone. The diabatic heating rate is ~ -0.5 K day^{-1} in the polar lower stratosphere. The upper stratospheric diabatic cooling is due to the dynamically induced warming resulting in enhanced longwave emission (Manzini et al. 2003; McLandress et al. 2010; Orr et al. 2012a). Motivated by this, we impose a diabatic perturbation between 150 and 30 hPa with the latitudinal dependence given by Eq. (1). The DIAB and DIAB5x simulations are also performed as an ensemble of branches starting on 1 October, and the diabatic heating perturbation is held constant in time with no seasonality. The effect of this diabatic cooling perturbation is explored both for a diabatic cooling perturbation similar in magnitude and location to the one due to ozone depletion (peaking at -0.5 K day^{-1}; DIAB simulation) and also a factor-of-5 larger (peaking at -2.5 K day^{-1}; DIAB5x simulation). Note that the net effect on the stratospheric vortex of the -0.5 K day^{-1} perturbation is slightly weaker than the corresponding ozone-hole-depletion run, as the -0.5 K day^{-1} perturbation is weakened by a negative feedback: cooler lower stratospheric temperatures lead to less longwave emission.

Table 1 summarizes all experiments included in this paper. For all integrations, the model is forced with CO_2 concentrations fixed at 390 ppmv and seasonally varying insolation. All simulations in this paper were run with a triangular truncation at wavenumber 42 (T42) with 40 vertical levels. All simulations use the identical settings for the gravity wave drag parameterization.

The climatological zonal mean wind in the PI integrations is shown in Fig. S1 in the online supplemental material for AQUA80 and STAT. The vortex breaks down more quickly in November in STAT due to the presence of additional tropospheric wave driving. In addition, the vortex is wider in AQUA80 and more meridionally confined in STAT, and hence the waveguide for Rossby waves into the stratosphere is better defined in STAT. We have performed additional experiments with the STAT configuration but in which the gravity wave flux was decreased so that the climatological November stratospheric vortex is stronger in STAT than in AQUA80. These additional simulations were used to assess sensitivity of the tropospheric response in STAT to the climatological stratospheric vortex strength. Results were quantitatively similar to those shown here (not shown).

3. Diagnostics

The role of synoptic and planetary waves in driving the poleward jet shift is diagnosed using the Eulerian mean zonal momentum budget:

$$\frac{\partial \overline{u}}{\partial t} = \underbrace{-\left[\frac{1}{a\cos^2\varphi}\frac{\partial}{\partial\varphi}(\cos^2\varphi\overline{u'v'}_{k\le 3}) + \frac{1}{\rho_0}\frac{\partial}{\partial z}(\rho_0\overline{u'w'}_{k\le 3})\right]}_{\text{eddy}_{1-3}}$$
$$\underbrace{-\left[\frac{1}{a\cos^2\varphi}\frac{\partial}{\partial\varphi}(\cos^2\varphi\overline{u'v'}_{k>3}) + \frac{1}{\rho_0}\frac{\partial}{\partial z}(\rho_0\overline{u'w'}_{k>3})\right]}_{\text{eddy}_{4+}}$$
$$+ \underbrace{f\overline{v}}_{\text{fv}} \underbrace{-\left[\overline{w}\frac{\partial\overline{u}}{\partial z} + \frac{\overline{v}}{a\cos\varphi}\frac{\partial}{\partial\varphi}(\overline{u}\cos\varphi)\right]}_{\text{advect}} + \overline{X} + \text{res} \quad (2)$$

(e.g., Andrews et al. 1987; Hitchcock and Simpson 2016), where the acceleration of the zonal-mean zonal wind on the left-hand side is contributed to by processes associated with (from left to right on the right-hand side): eddy momentum

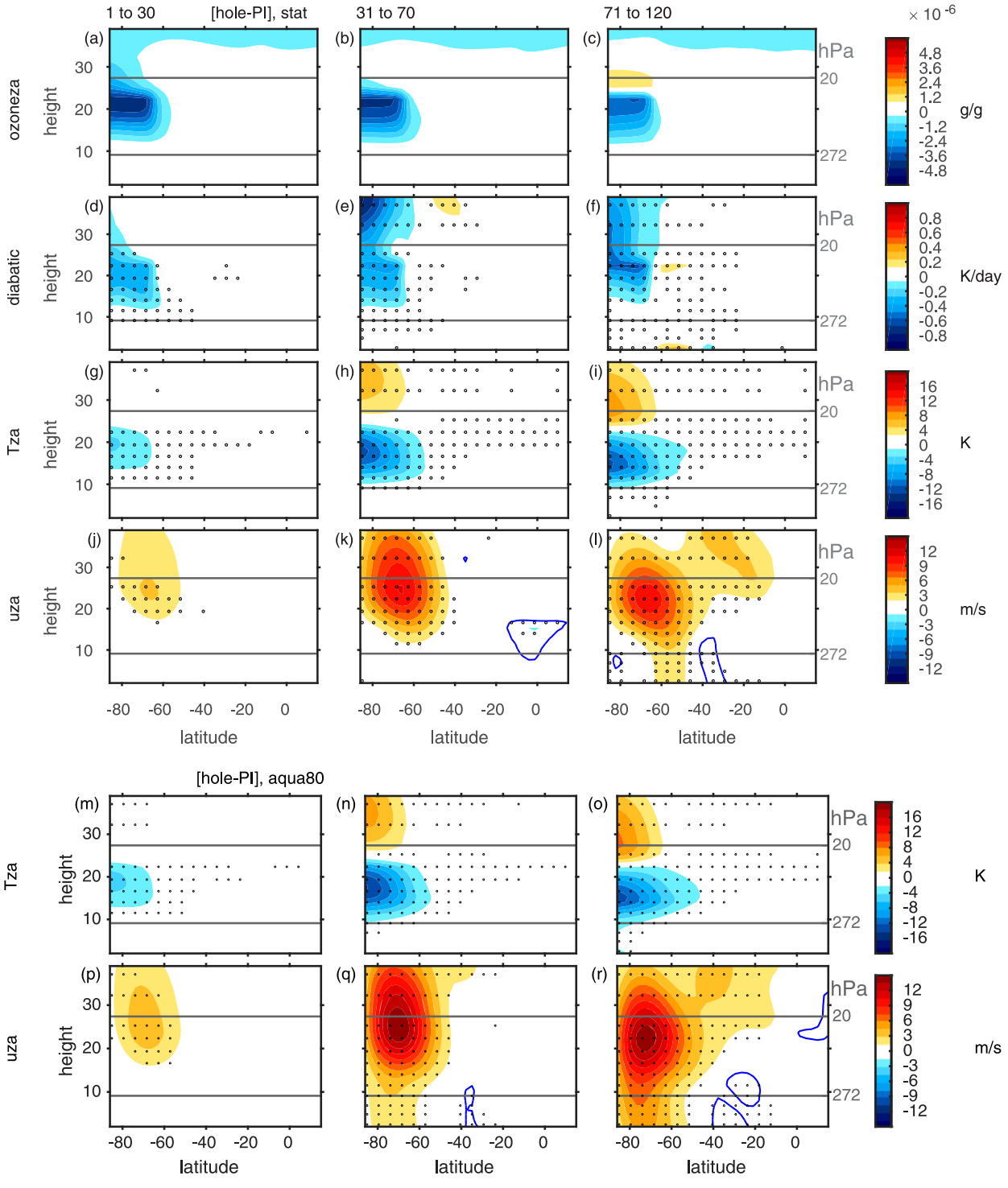

FIG. 1. Zonal-mean responses to ozone loss [i.e., ozone hole minus preindustrial (PI)] in the most realistic configuration, STAT, in (left) days 1–30 after branching, i.e., October; (center) days 31–70, i.e., Nov and 1–10 Dec; and (right) days 71–120, i.e., 11 Dec–30 Jan for (a)–(c) ozone perturbation; (d)–(f) diabatic heating rate computed as the sum of the temperature tendency due to longwave, shortwave, and latent heat release; (g)–(i) temperature; and (j)–(l) zonal wind. (m)–(r) As in (g)–(l), but for an aquaplanet configuration with Antarctic albedo = 0.8. Stippling indicates anomalies that are statistically significant at the 95% level. For the zonal wind responses, the -0.75 m s^{-1} contour is shown in blue.

TABLE 1. MiMA experiments, with "Y" indicating that a forcing is on and "N" indicating that a forcing is off. For ozone, we compare a "preindustrial" simulation using ozone concentrations from the CMIP6 read-in file over the years 1860–99 with a simulation using ozone concentrations from the CMIP6 read-in file over the years 1990–99, which were then modified in the Antarctic lower stratosphere (see section 2) to capture a deeper ozone hole evident in some years. The November SH jet latitude and January annular mode time scale (in days) in the PI integration are included. For STATNH, the annular mode time scale is shown for May in the Northern Hemisphere; in April, the time scale is 24 days.

	Perturbation	Surface zonal structure	Antarctica albedo	Nov jet lat	AM time scale
STAT, ozone hole − PI	Ozone loss	Y	0.8	47.7S	37
AQUA80, ozone hole − PI	Ozone loss	N	0.8	46.5S	43
AQUA27, ozone hole − PI	Ozone loss	N	0.27	43.1S	50
STATNH, ozone hole − PI	Ozone loss	Y	0.8		23
STAT, DIAB − PI	Diabatic 1x	Y	0.8	47.7S	37
AQUA80, DIAB − PI	Diabatic 1x	N	0.8	46.5S	43
STAT, DIAB5x − PI	Diabatic 5x	Y	0.8	47.7S	37
AQUA80, DIAB5x − PI	Diabatic 5x	N	0.8	46.5S	43

flux convergence due to planetary waves (eddy_{1-3}), eddy momentum flux convergence due to synoptic waves (eddy_{4+}), Coriolis torques acting on the meridional motion (fv), mean flow momentum advection (advect), and parameterized processes including the zonal wind tendency due to vertical and horizontal diffusion and gravity wave drag in the model ($\overline{X}$). All variables follow standard notation (e.g., see Andrews et al. 1987). The final term (res) is the budget residual and is contributed to by issues associated with sampling and truncation errors.

Previous work has linked the climatological position of the jet, the Southern Annular Mode (SAM) time scale, and the amplitude of the jet response to polar stratospheric perturbations (e.g., Garfinkel et al. 2013). The SAM and the *e*-folding time scale of the corresponding principal component time series are computed following the methods of Baldwin et al. (2003) and Gerber et al. (2008). Jet latitude is computed by fitting the 850-hPa zonal mean zonal wind near the jet maxima (as computed at the model's T42 resolution) to a second-order polynomial, and then evaluating the polynomial at a meridional resolution of 0.12°. The latitude of the maximum of this polynomial is the jet latitude (Garfinkel et al. 2013).

4. The response to an identical ozone perturbation with and without stationary waves

We begin by showing that in the STAT configuration of MiMA, ozone loss leads to impacts similar to those shown in previous works using reanalysis or comprehensive models. Figure 1g–i shows the temperature response to reduced ozone. Temperatures in the polar lower stratosphere gradually decrease over the first two months and reach −15 K by November, and the anomaly propagates downward to near the tropopause in late December (Fig. 1i). This cooling is similar to that observed during years with a particularly strong ozone hole relative to 1960s conditions (Randel et al. 2009; Previdi and Polvani 2014). The zonal wind response is shown in Figs. 1j–l, and captures the response evident in reanalysis, CMIP, and CCMI data (Previdi and Polvani 2014; Son et al. 2018).

The spatial distribution of ozone-induced tropospheric circulation changes is illustrated in Fig. 2. As anticipated from Figs. 1j–l, changes in 500-hPa geopotential height resemble the canonical SAM pattern (Figs. 2b,c; Kidson 1988; Thompson and Wallace 2000; Thompson et al. 2011) with lower heights in subpolar latitudes and higher heights between 40° and 50°S. The model also simulates the precipitation response to ozone depletion unlike dry models used in many mechanistic studies. Figures 2d–f show an increase in precipitation over eastern Australia and southeastern South America and drying over New Zealand (in agreement with observed trends; Hendon et al. 2007; Ummenhofer et al. 2009; Gonzalez et al. 2014). Such precipitation changes are consistent with a poleward shift of the jet.

The increase in subpolar zonal wind peaks near day 75 at 77 hPa (15 December; Fig. 3a), although higher in the stratosphere the response peaks earlier, and is followed by a zonal wind and SAM response in the troposphere (Fig. 3b for 850-hPa wind and Fig. 3c for geopotential height). While a tropospheric response begins to develop in November, it does not project onto a classical SAM pattern but rather is an acceleration of winds on the subpolar flank of the jet similar to the responses in White et al. (2020, 2022). Only in December (and then intensifying into early January) do the wind anomalies resemble a dipole flanking the climatological jet as seen in previous work.

Encouraged by the quantitative accuracy of the response in the most realistic configuration, we now take advantage of the flexibility of the idealized model in order to understand the role of stationary waves for the surface response. As discussed in section 2, the same ozone perturbation has also been imposed in two aquaplanet configurations of the model (differing only in the polar albedo) and in the Northern Hemisphere. We begin with the aquaplanet configuration with a polar albedo of 0.8 (AQUA80), as this turns out to be the tropospheric configuration with the largest surface response to ozone depletion, with other configurations discussed later. Even though the ozone perturbations are identical, the wind response (Fig. 1, bottom row) is larger in AQUA80[1] and the

[1] STAT features enhanced surface drag over Antarctica as compared with AQUA80, likely explaining some of the enhanced response in AQUA80 (see Fig. S2 in the online supplemental material); however, the response is stronger in the stratosphere as well as in midlatitudes where the specification of surface drag is identical.

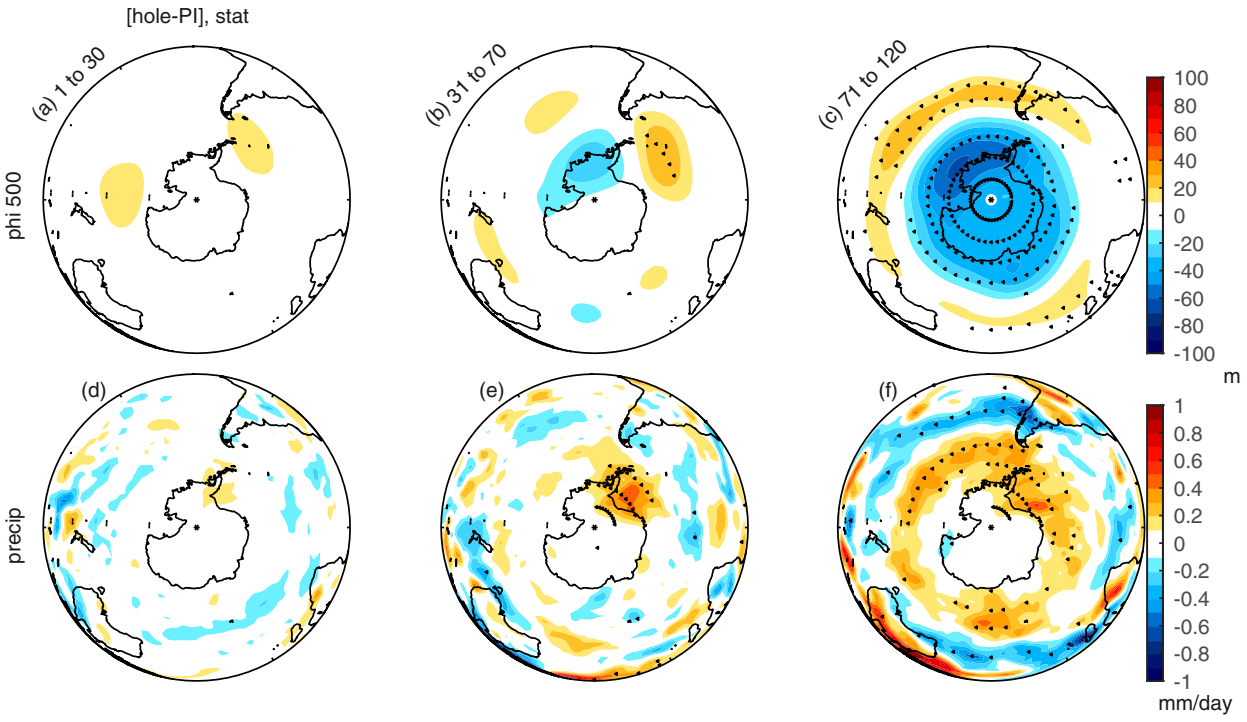

FIG. 2. Map view of ozone loss response (ozone hole − PI) in the most realistic configuration in (left) days 1–30 after branching, i.e., October; (center) days 31–70; and (right) days 71–120 for (a)–(c) geopotential height at 500 hPa and (d)–(f) precipitation. Stippling indicates anomalies that are statistically significant at the 95% level.

cooling of the polar lowermost stratosphere is also ~20% larger in AQUA80. The difference in zonal wind response between the two configurations is statistically significant at the 5% level after day 30 in both the stratosphere and troposphere (Fig. 4c). The geopotential height response in the troposphere to ozone loss is more than twice as large in AQUA80 as in STAT (Figs. 2a–c vs Figs. 5a–c, and Fig. 3c vs Fig. 6c), and the precipitation response is also more extensive due to the lack of Antarctic orography (Figs. 5d–f). The difference in response is evident both in November and in December/January (Fig. 4c).

5. Why do stationary waves reduce the amplitude of the response?

To answer this question, we explore the impacts of stationary and transient planetary waves on the jet response to ozone loss and equivalent diabatic cooling anomalies.

a. Stationary waves negatively feed back on the jet shift response

Even though the ozone perturbation is identical in STAT and AQUA80, ozone depletion leads to less stratospheric vortex strengthening and polar cap cooling in STAT relative to AQUA80 (Figs. 1 and 4c) due to the presence of stationary waves. This difference in response to an identical ozone perturbation occurs because the strengthened vortex in late spring and early summer (e.g., November and December) due to ozone depletion favors more upward wave propagation. The subsequent enhanced wave convergence within the stratosphere leads to dynamical warming of the polar cap via downwelling of the vertical wind of the residual circulation. This cancels a part of the radiatively driven cooling near the tropopause (Manzini et al. 2003; Li et al. 2010; McLandress et al. 2010; Orr et al. 2012a; Figs. 1d–i). However, this increase in upward propagating waves is more dramatic in the presence of stronger wave forcing from below, and in STAT these upward propagating waves are indeed stronger due to the presence of stationary waves forced by the bottom boundary.

We demonstrate this effect in Fig. 4d, which shows the vertical component of the Eliassen–Palm (EP_z) flux at 40 hPa; other levels in the mid- and lower stratosphere exhibit a similar response (Fig. S3 in the online supplemental material). In STAT (blue line), an ozone hole leads to increased upward wave flux by late October, and the anomaly stays positive throughout the duration of the run. The increase in AQUA80 is weaker however (black line), and the difference between STAT and AQUA80 is statistically significant between days 75 and 90, although if we time average in, say, 10-day chunks, the signal emerges from the noise after day 30. The net effect is a warmer polar stratosphere and less accelerated vortex in STAT (Fig. 4c). Hence, stationary waves act as a negative feedback on the stratospheric response to ozone, acting to partially offset the ozone-induced cooling, and thus partially mitigate the poleward tropospheric jet shift.

We demonstrate this further by comparing the Eulerian mean eddy driving term for AQUA80 as compared with STAT. Figures 7a–c and 8a–c decompose this eddy forcing into its wave-1 component for AQUA80 and STAT respectively. Recall that wave 1 is the dominant zonal wavenumber of stationary

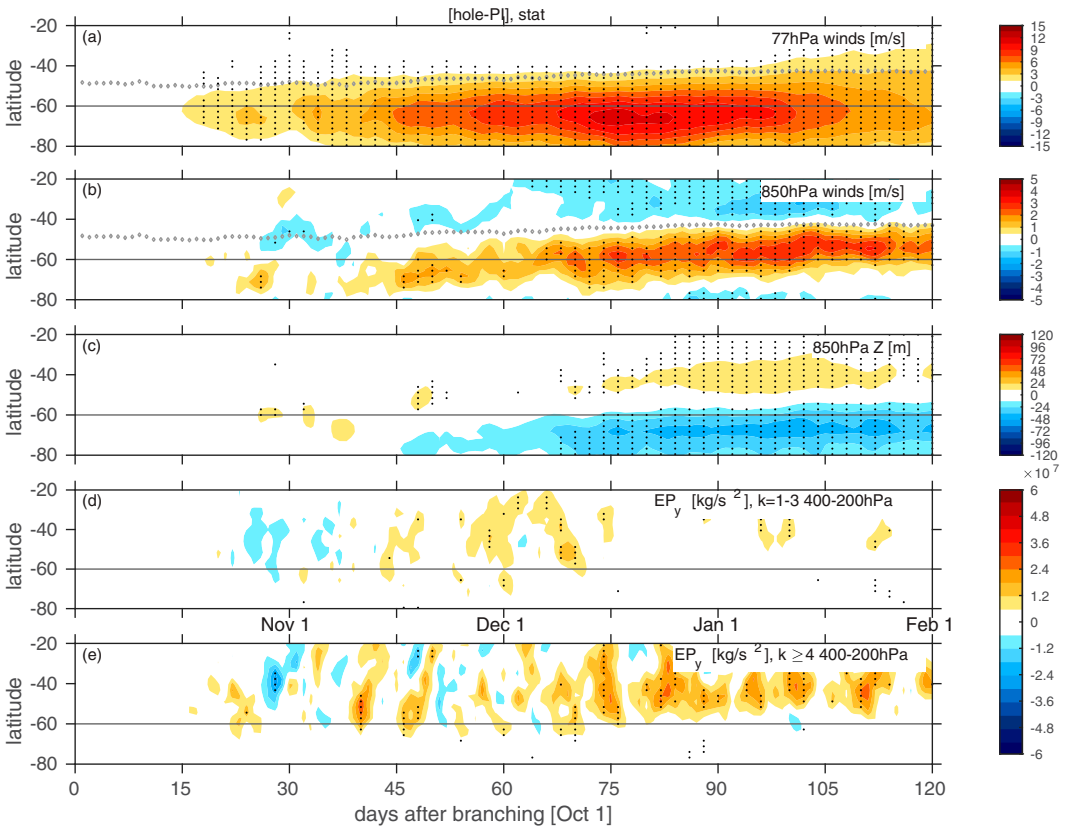

FIG. 3. Development and downward propagation of the response to the ozone perturbation in the most realistic configuration: (a) 77-hPa zonal wind, (b) 850-hPa zonal wind, and (c) 850-hPa polar cap geopotential height, as well as upper-tropospheric meridional Eliassen–Palm flux due to (d) planetary and (e) synoptic waves. The tropospheric jet latitude is shown in (a) and (b) with gray diamonds. Stippling indicates anomalies that are statistically significant at the 95% level.

waves in STAT and in reanalysis data (Garfinkel et al. 2020a). In STAT, wave 1 acts to weaken the vortex even as ozone depletion is strengthening it; however, in AQUA80 wave 1 (which is composed of transient waves only) is associated with a net strengthening of the vortex. Results are similar if the transformed Eulerian mean (TEM) is used as well (Figs. S3 and S4 in the online supplemental material), with the anomalies in wave-1 EP_z and subpolar stratospheric EP flux divergence resembling an amplified version of those present in the climatology. This amplification of climatological wave-1 EP_z and EP flux divergence leads to a stronger vortex response in AQUA80 than in STAT to the same ozone perturbation.

This negative feedback caused by the presence of stationary waves can be further demonstrated by imposing the ozone perturbation in the Northern Hemisphere. The stratospheric wind and temperature responses are clearly much weaker (Fig. S5 in the online supplemental material) and no longer robustly extend into the troposphere. We quantify the relationship between the subpolar zonal wind responses to ozone depletion in the lower stratosphere and lower troposphere in Fig. 9, which compares the response of subpolar zonal wind in the (y axis) lower stratosphere and (x axis) lower troposphere. The blue line shows the response in STAT in the SH: the average wind anomaly for days 61–75 is 7.8 m s^{-1} at 77 hPa and 1.2 m s^{-1} at 850 hPa; in contrast, in AQUA80 the wind responses are stronger (black; 9.5 m s^{-1} at 77 hPa and 2.0 m s^{-1} at 850 hPa). The corresponding changes for the NH (in green) are much weaker both in the lower stratosphere and troposphere despite cooling aloft (3.3 and 0.3 m s^{-1} respectively). The net effect is that stationary waves, of which there is more activity in the NH, help dampen the surface response to ozone depletion.

b. *Transient planetary waves encourage the jet response*

Even though stationary planetary waves dampen lower stratospheric cooling and thus the surface response, we now show that transient planetary waves do the opposite: they contribute positively to the surface response in agreement with Smith and Scott (2016). We demonstrate this by considering the Eulerian mean momentum budget for AQUA80, which captures only transient planetary waves by design. The zonal wind tendency calculated explicitly is shown in Figs. 10a–c, and the various terms in the budget [Eq. (2)] are shown in the rest of Fig. 10. Figures 10d–f show the sum of all terms on the right-hand size of Eq. (2), which should be equal to the zonal wind tendency in Figs. 10a–c. This is indeed the case: the budget closes in nearly all regions, although some of the fine-scale

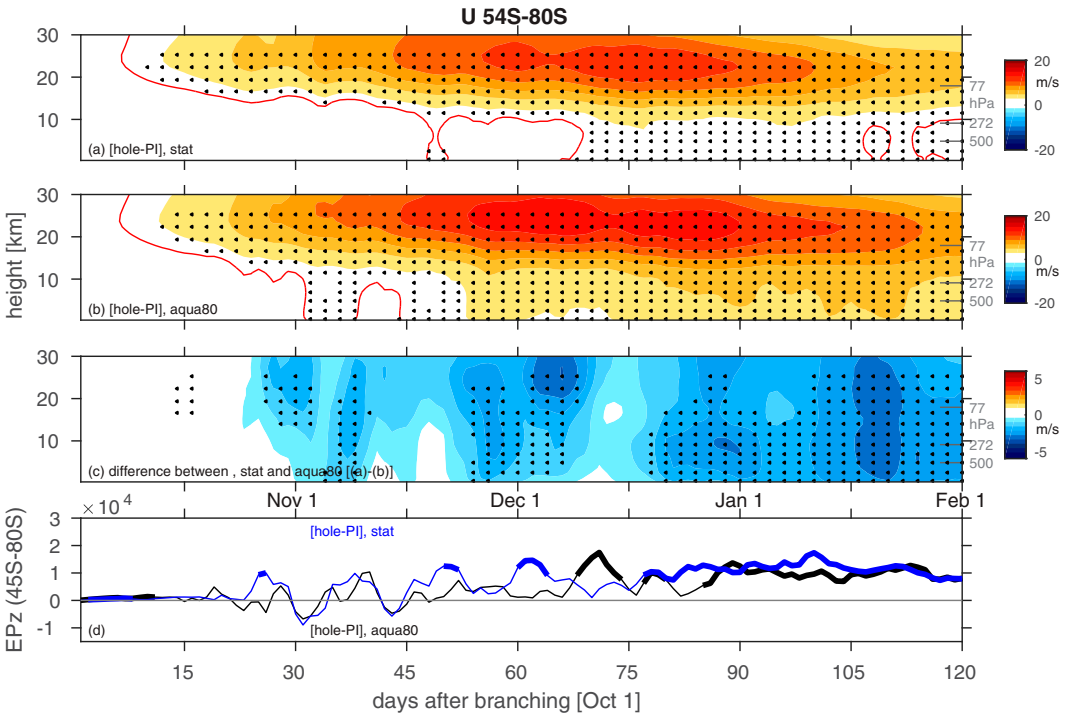

FIG. 4. Evolution of zonal wind from 54° to 80°S for the ozone hole − PI runs with (a) realistic stationary waves (STAT) and (b) an aquaplanet, with Antarctic albedo equal to 0.8 (AQUA80). (c) The difference between (a) and (b). The contour interval is 2 m s^{-1} in (a) and (b) and 0.5 m s^{-1} in (c). The 1 m s^{-1} contour is indicated in red in (a) and (b). Stippling indicates anomalies that are statistically significant at the 95% level. (d) Vertical component of the EP flux at 40 hPa, area-weighted average from 80° to 45°S (kg s^{-2}), with a thick line denoting a significant response to ozone.

details of the wind tendencies differ due to truncation errors in the calculations.

The dominant terms are the eddy forcing term (Figs. 10g–i) and the Coriolis torque (Figs. 10j–l), with the acceleration in most regions and time periods provided by the eddy forcing term. The sum of the eddy forcing and Coriolis terms (Figs. 10m–o) captures the bulk of the total tendency in most regions/time periods (Figs. 10d–f), but crucially in the mid- and upper stratosphere changes in gravity wave absorption act as a negative feedback in days 31–70 (late spring) and dominate the response in days 71–120 (summer). The zonal wind anomaly peaks in December before weakening in January and February because the already accelerated vortex allows for more gravity wave absorption above the midstratosphere. The advection term also contributes in regions with strong wind gradients (Figs. 10s–u). The net effect is that the dominant term for the subpolar zonal acceleration is the resolved eddy term in Figs. 10g–i, and importantly this wave-induced acceleration extends from the stratosphere to below the tropopause. A similar interpretation is reached using the TEM budget (Fig. S6 in the online supplemental material).

Figure 7 decomposes the eddy forcing into its wavenumber components. At early lags, the subpolar tropospheric response arises mostly through wave 2 and wave 3 (Figs. 7d–f), while for days 71–120 synoptic wavenumbers are most important at all latitudes (Figs. 7g–i). The wave 2 and wave 3 present in AQUA80 are transient planetary waves, and it is clear that they help to set up the initial jet shift and then contribute a continued acceleration at subpolar latitudes. Wave 1 does not contribute to forcing the jet shift (Figs. 7a–c). These conclusions are true of the STAT runs as well (Fig. 8) despite observed and STAT SH stationary waves being dominated by wave 1 (Garfinkel et al. 2020a), leading to a different stratospheric response of wave 1 to ozone depletion (Figs. 7a–c vs Figs. 8a–c). Thus, the stratospheric wave-1 response is not of direct relevance for the tropospheric jet shift.

The importance of both planetary and synoptic waves is also evident using the TEM budget [as in Orr et al. (2012b)]. The time evolution of the upper tropospheric (200–400 hPa) meridional component of the EP flux (EP_y) in response to ozone loss is shown in Figs. 3d,e and 6d,e for STAT and AQUA80; both synoptic and planetary waves are important. The timing of the increase in EP_y is similar for both synoptic and planetary waves, however, and thus it is unclear if one can be argued to help induce the other. That being said, these figures (and also Fig. 7) show that, at later lags, synoptic wavenumbers dominate the response. A similar relative role for planetary waves versus synoptic waves for the tropospheric jet shift is evident for both AQUA80 and STAT in response to ozone loss (in both Figs. 3d,e and 6d,e), and hence the presence of stationary waves does not appear to affect the ability of planetary waves to contribute to the jet shift. However the jet shift is weaker for STAT (due to a weaker stratospheric response as discussed above) and consistent with this the overall eddy forcing is weaker too (Figs. 3d,e vs Figs. 6d,e).

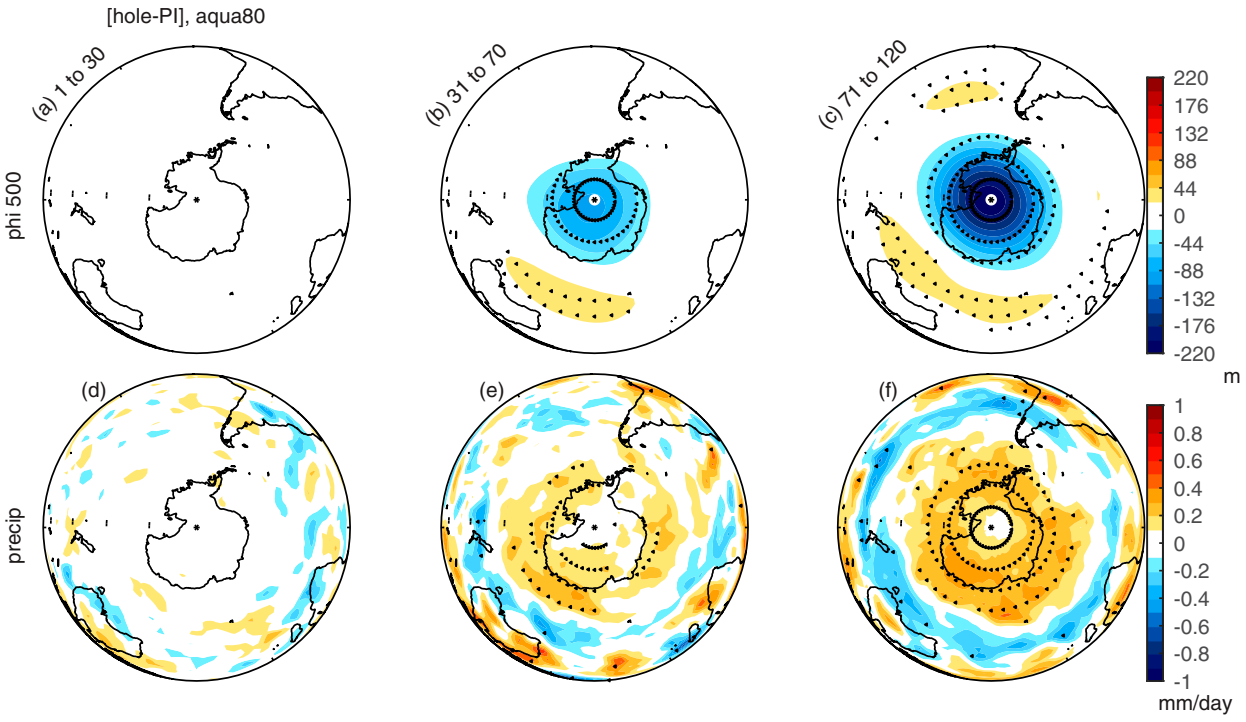

FIG. 5. As in Fig. 2, but for an aquaplanet configuration with Antarctic albedo = 0.8. Note that the color scale for the top row differs from Fig. 2. Continental outlines are included for reference only.

c. *Linearity of response and comparison of stratospheric diabatic heating with ozone loss*

In addition to the ozone-hole runs presented thus far, we have also performed integrations in which a diabatic cooling perturbation replaces the ozone perturbation. As discussed in section 2, the spatial structure of the diabatic cooling perturbation follows the ozone perturbation, and its magnitude (-0.5 K day^{-1}) mimics that due to ozone depletion (Figs. 1d–f). The benefits from these diabatic cooling runs are twofold: first, we can increase the amplitude of this diabatic cooling perturbation at will and hence explore the linearity of the response. (In contrast, the impact of ozone saturates as concentrations cannot be negative.) Second, there is no shortwave heating perturbation by construction as ozone is unchanged [the effects of UV on the surface energy budget discussed in Chiodo et al. (2017) are turned off], and hence the stationary waves present in STAT but absent in AQUA80 are the only factor that can lead to a difference in the surface response.

We begin with the linearity of the response. Figure 9b is similar to Fig. 9a, but showing the response to a diabatic cooling perturbation imposed on STAT and AQUA80 (STAT DIAB-PI and AQUA80 DIAB-PI on Table 1). By construction, the lower stratospheric and tropospheric wind response for a -0.5 K day^{-1} perturbation (the dark purple and dark gray lines) in Fig. 9b resemble qualitatively their counterpart in Fig. 9a. The experiments with a factor-of-5 stronger perturbation (-2.5 K day^{-1}) are also shown in Fig. 9b, but with the subsequent response divided by a factor of 5. It is clear that the response is fairly linear, consistent with White et al. (2020), who find a generally linear response to short-lived but stronger thermal perturbations. Note that the response in AQUA80 is slightly weaker than might be expected by linearity, although the response for STAT is stronger. This result highlights the fact that interannual variability in ozone concentrations should be useful for seasonal predictability of surface climate (Son et al. 2013; Bandoro et al. 2014; Hendon et al. 2020; Jucker and Goyal 2022; Oh et al. 2022).

Next, we use these diabatic forcing experiments to isolate the role of stationary waves for the downward response, as these experiments do not allow for any perturbation of shortwave radiation on the surface by ozone. The subpolar zonal wind response for STAT and AQUA80 to an identical diabatic perturbation is shown in Figs. 11a and 11b, and the difference between the two is in Fig. 11c. The diabatic perturbation causes a larger zonal wind response in AQUA80 in both the stratosphere and troposphere after day 30. Hence, stationary waves lead to a negative feedback on the response even if surface shortwave effects are suppressed, as diagnosed by the TEM momentum budget in Fig. S7 in the online supplemental material. Note that for the diabatic experiments the EP flux anomalies also resemble an amplification of the climatological EP flux (Fig. S4 in the online supplemental material). Overall, these results support the conclusion of Chiodo et al. (2017) that shortwave surface effects are not important for the tropospheric response in austral summer.

6. The role of surface cooling and jet latitude/persistence

Surface temperature over Antarctica cools in response to ozone depletion (Grise et al. 2009; Yang et al. 2014;

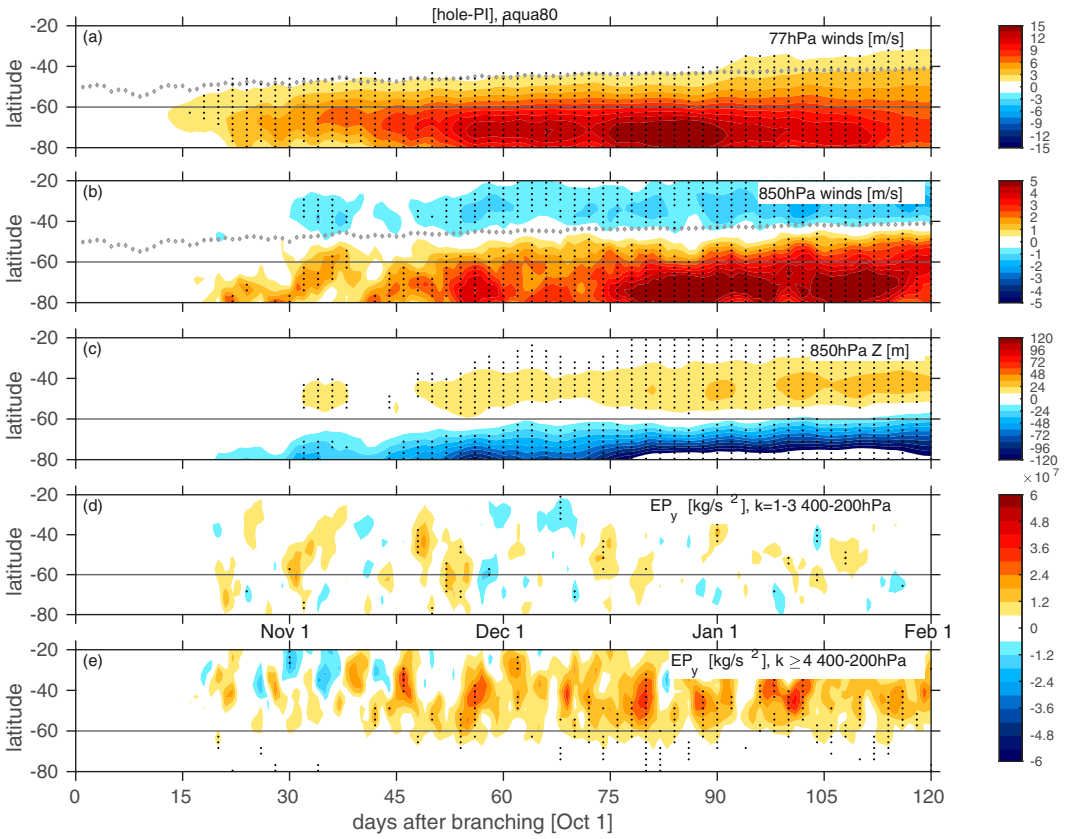

FIG. 6. As in Fig. 3, but for aquaplanet with Antarctic albedo = 0.8.

Previdi and Polvani 2014), and while much of this change is likely due to the shift of the jet (or equivalently, the shift toward a positive SAM index), this cooling can still feed back onto the jet shift. We now use the idealized model to isolate the impacts of the surface temperature change on the jet.

Recall that the albedo in both AQUA80 and STAT is 0.8 over Antarctica and 0.23 elsewhere. To disentangle the role of the surface temperature changes over Antarctica on the jet shift, we have performed an additional aquaplanet integration with an albedo of 0.27 everywhere (AQUA27). AQUA80 and AQUA27 differ only in the specification of albedo; by summer, surface temperatures rise over Antarctica by 1 K due to enhanced shortwave absorption in AQUA27, rather than cooling by 4 K as in AQUA80 (Fig. 12d). The warmer near-surface tropospheric polar cap in AQUA27 leads to higher geopotential height throughout the column, as can be quantified using the hypsometric equation (not shown). The net effect is that the meridional gradient in geopotential is more extreme in AQUA80 than in AQUA27, and thus the stratospheric zonal wind response and tropospheric jet shift (Figs. 12a–c) are stronger in AQUA80. In other words, the polar surface cooling in AQUA80 reinforces the ozone-induced poleward shift, and hence provides a positive feedback.

Son et al. (2010) and Garfinkel et al. (2013) found that the tropospheric response to an identical polar stratospheric diabatic perturbation is sensitive to jet latitude and jet persistence, with jets closer to 40°S more persistent and more sensitive to stratospheric perturbations. This finding is apparently contradicted by the responses in AQUA27 and AQUA80: the response is weaker in AQUA27 relative to that in AQUA80 even as the jet latitude is closer to 40°S and the annular mode time scale of the SAM is slightly longer in AQUA27 (Table 1). This indicates that the surface temperature effect in AQUA27 overwhelms the jet latitude/eddy feedback strength effect.[2]

To cleanly assess the eddy feedback strength effect highlighted by Garfinkel et al. (2013), we have performed an experiment using the AQUA80 configuration but in which the jet is pushed ~7° farther poleward. This is achieved by imposing a stronger and more poleward meridional ocean heat transport gradient following Eq. (A8) of Garfinkel et al. (2020a) with an amplitude of 50 W m^{-2},

[2] Note that jet latitude in STAT is poleward of that in AQUA80 by 1.2° (Table 1), whereas the annular mode time scale is slightly shorter in STAT, likely because stationary waves act to interfere with eddy feedback. While this slightly weaker eddy feedback may explain part of the weaker tropospheric response in STAT, it cannot explain the weaker stratospheric response. Note also that the polar surface cooling in AQUA80 is not present in STAT (consistent with the opposite-signed surface temperature anomalies associated with the SAM in the preindustrial control run of each configuration; see Fig. S9 in the online supplemental material), which also may explain some of the weakened response in STAT.

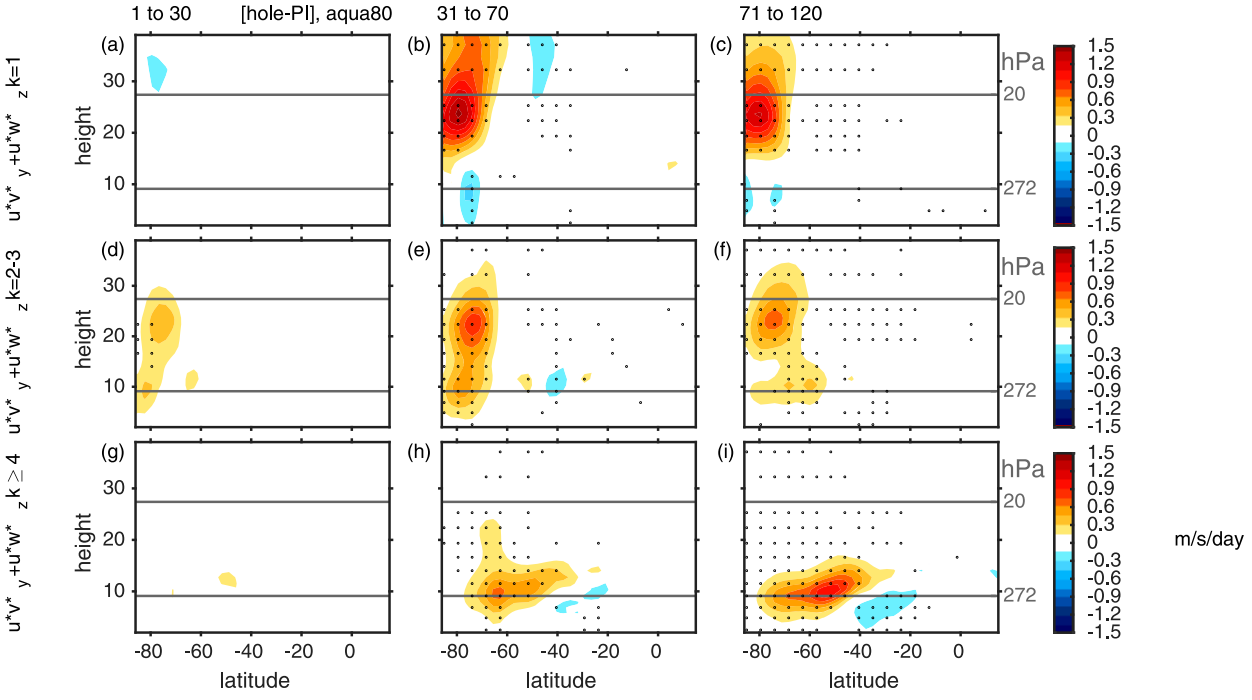

FIG. 7. Decomposition of the eddy forcing term in Figs. 10g–i into the various wavenumber components: (a)–(c) wavenumber 1, (d)–(f) wavenumbers 2 and 3, and (g)–(i) wavenumbers 4 and larger. The difference between AQUA80 ozone hole and AQUA80 PI is shown.

which leads to a poleward shift of the sea surface temperature gradient. The response to ozone depletion is shown in Fig. S8 in the online supplemental material, and it is clear that the tropospheric response is weaker, as expected. Both integrations lack stationary waves, and the surface shortwave effects are identical. Hence the weakened tropospheric response must be due to jet latitude and weakened eddy feedback.

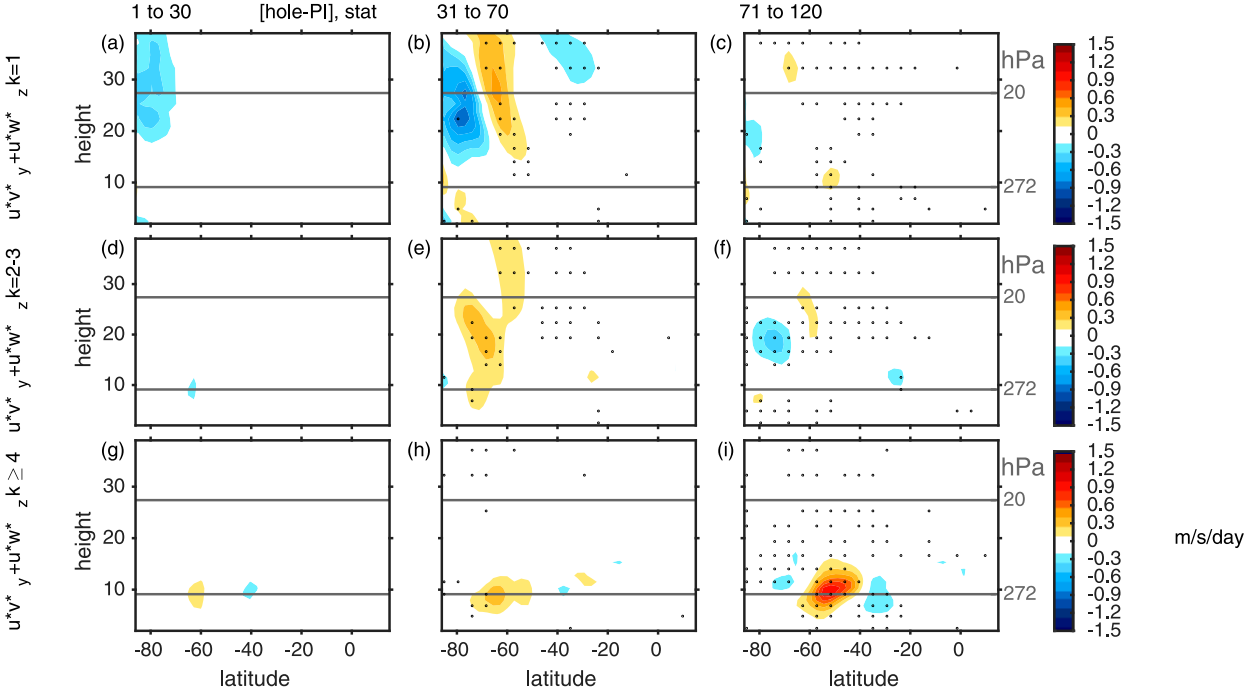

FIG. 8. As in Fig. 7, but for the difference between STAT ozone hole and STAT PI.

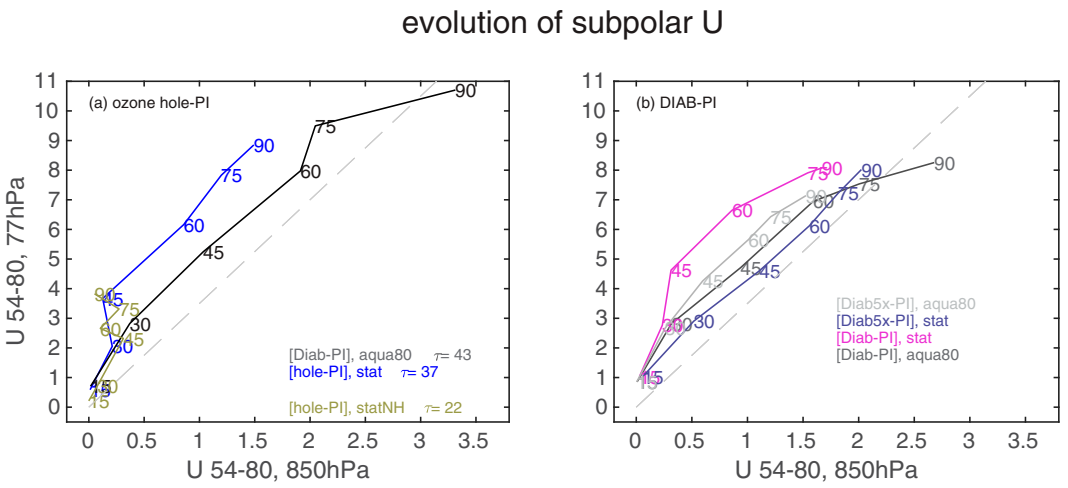

FIG. 9. Evolution of subpolar U for the (a) ozone hole − PI runs with realistic stationary waves (blue), an aquaplanet with Antarctic albedo equal to 0.8 (black), and Northern Hemisphere with realistic stationary waves (green). (b) Runs analogous to ozone hole − PI but in which a diabatic cooling perturbation is imposed directly. The mean of each 15-day segment after branching is indicated with a dot and is labeled by the last day included in the 15-day segment (e.g., 30 is for days 16–30). For (b), for the runs with a factor-of-5 increase in diabatic cooling rate, we divide the response by a factor of 5. A dashed gray line indicates a constant reference slope of 3.5.

This run includes a stronger sea surface temperature front than AQUA80 yet has a weaker response, apparently contrary to Ogawa et al. (2015), who find that a stronger sea surface temperature front leads to a stronger response. However, our results and those of Ogawa et al. (2015) can be reconciled if one focuses on the eddy feedback strength: in both papers a stronger eddy feedback strength leads to a stronger response, and the difference in the specification of the sea surface temperature front leads to a different effect on eddy feedback. Hence, the results of Ogawa et al. (2015) may have more to do with the eddy feedback strength in their simulations than the well-defined sea surface temperature front.

7. Discussion and conclusions

Ozone depletion is known to have been the dominant contributor to a poleward shift of the Southern Hemisphere tropospheric midlatitude jet, precipitation, and storm tracks over the late twentieth century. Over the next 50 years, ozone recovery is expected to nearly cancel out changes in the jet and Hadley cell that would otherwise be forced by greenhouse gases (Polvani et al. 2011a; Arblaster et al. 2011; Barnes and Polvani 2013; Gerber and Son 2014; Waugh et al. 2015; Seviour et al. 2017; Son et al. 2018; Banerjee et al. 2020). The degree of cancellation is uncertain and model dependent, however, leading to uncertainty in future projections (Gerber and Son 2014). The mechanism whereby ozone depletion leads to a downward impact, and the details of how this mechanism governs the magnitude of the impact, are still unclear (as noted in the WMO ozone assessments in 2010, 2014, and 2018). While previous work has shown that jet latitude (Garfinkel et al. 2013) and the details of the ozone forcing (Neely et al. 2014; Young et al. 2014) are important, we have demonstrated two additional processes that regulate the magnitude of the downward impact: surface cooling and stationary waves.

This study takes advantage of an intermediate-complexity model that can delineate the role of these two effects. We integrate it with realistic stationary waves, comparing it with runs without any zonal asymmetry in the bottom boundary. For both configurations of the bottom boundary, we compare integrations with an ozone hole, in which surface shortwave feedbacks are present, with integrations with a diabatic temperature tendency that mimics the shortwave effects of ozone depletion in the stratosphere only. By comparing these runs, we isolate the role of stationary waves for the surface response, and demonstrate that the response is 2 times as strong for many of the diagnostics examined when no stationary waves are present (Figs. 1m–o, 5, 6, and 11a,b). We find a quantitatively similar effect if the gravity wave settings in STAT are changed so that the vortex in STAT is stronger than that in AQUA80, and hence the stratospheric vortex climatological strength is not a leading-order factor.

The presence of stationary planetary-scale waves leads to a weaker response to an identical diabatic cooling perturbation starting in November and extending into February. This effect arises because stationary waves negatively feedback on the imposed stratospheric perturbation and weaken it if stationary waves are forced by the bottom boundary. That is, as the vortex strengthens it allows more upward wave activity into the stratosphere, and this reservoir of wave activity is larger if stationary waves are present. Even though Southern Hemisphere stationary waves are weaker than their Northern Hemisphere counterpart, they nonetheless are crucial for regulating the net response to ozone depletion.

We demonstrate that surface radiative effects are not critical for the tropospheric response, in agreement with

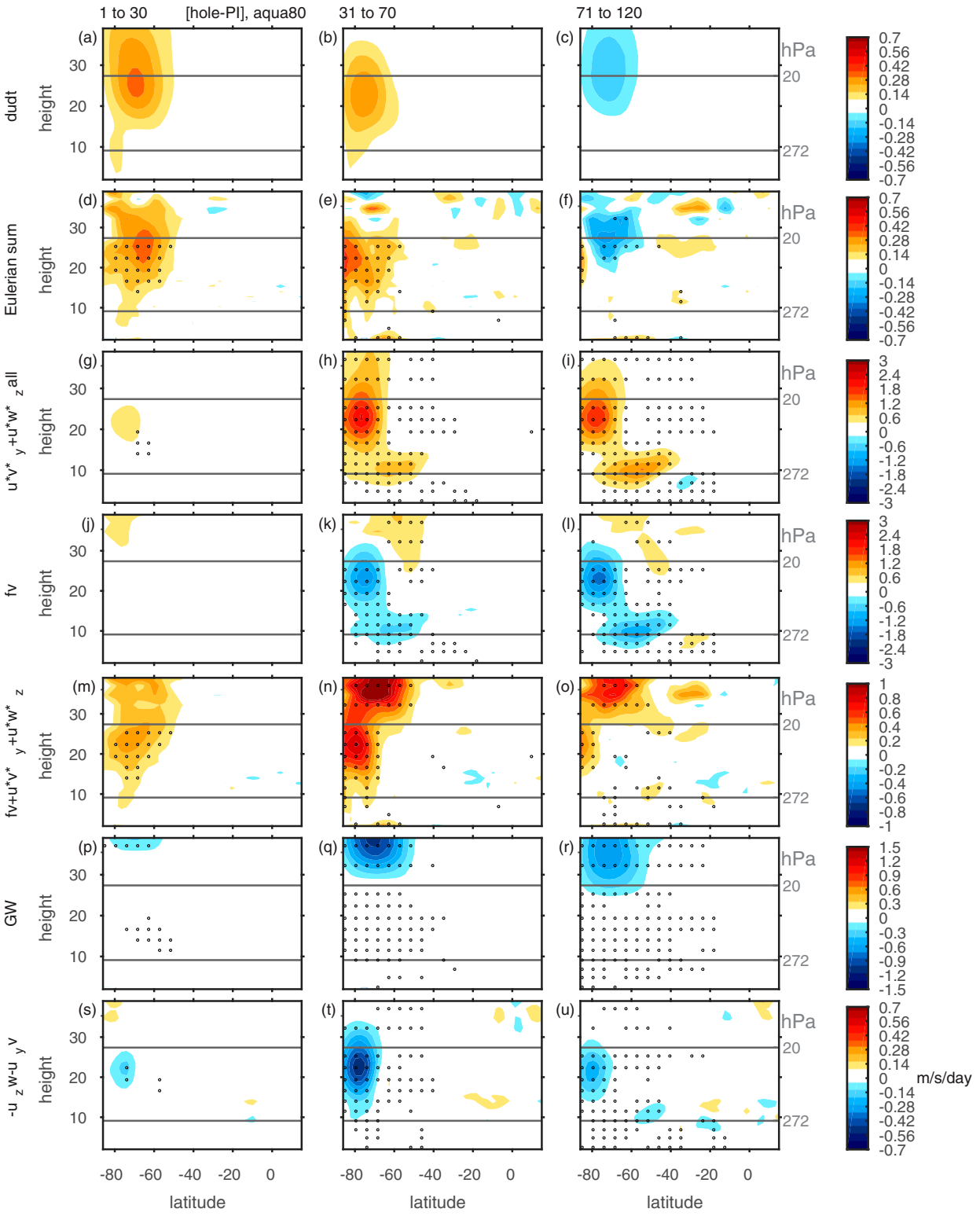

FIG. 10. Eulerian mean momentum budget for the ozone hole − PI aquaplanet runs, with Antarctic albedo equal to 0.8 in (left) days 1–30 after branching, i.e., October; (center) days 31–70; and (right) days 71–120 for (a)–(c) total wind tendency, (d)–(f) the sum of all terms, (g)–(i) the eddy forcing terms ($u'v'$ and $u'w'$), (j)–(l) Coriolis torque, (m)–(o) the sum of eddy forcing and Coriolis torque, (p)–(r) gravity wave drag, and (s)–(u) advection of mean zonal wind. Note that the color bars for (g)–(i) and (j)–(l) differ from that in (m)–(o) due to the strong cancellation between eddy forcing and Coriolis torque (as expected).

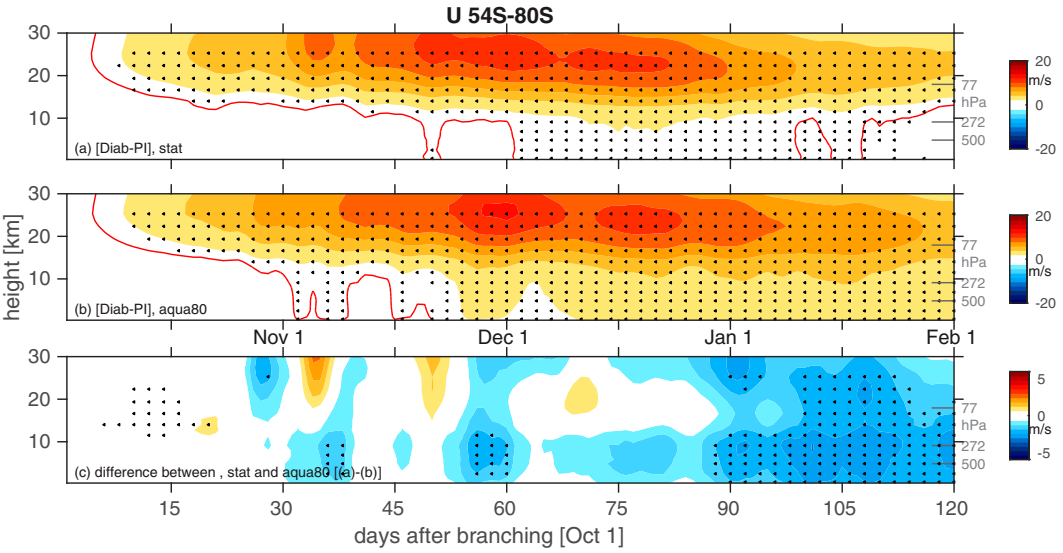

FIG. 11. Evolution of zonal wind from 54° to 80°S for the Diabatic − PI runs with (a) realistic stationary waves and (b) an aquaplanet with Antarctic albedo equal to 0.8. (c) The difference between (a) and (b). The 1 m s^{-1} contour is indicated in red in (a) and (b).

Chiodo et al. (2017), by contrasting the response to ozone depletion versus an equivalent stratospheric diabatic cooling perturbation (Fig. 9). While surface radiative effects are not important, the surface temperature response does contribute to the magnitude of the jet shift. Specifically, by integrating the model in an aquaplanet configuration but with different surface albedos over Antarctica, we isolate the role of surface temperature and showed that surface

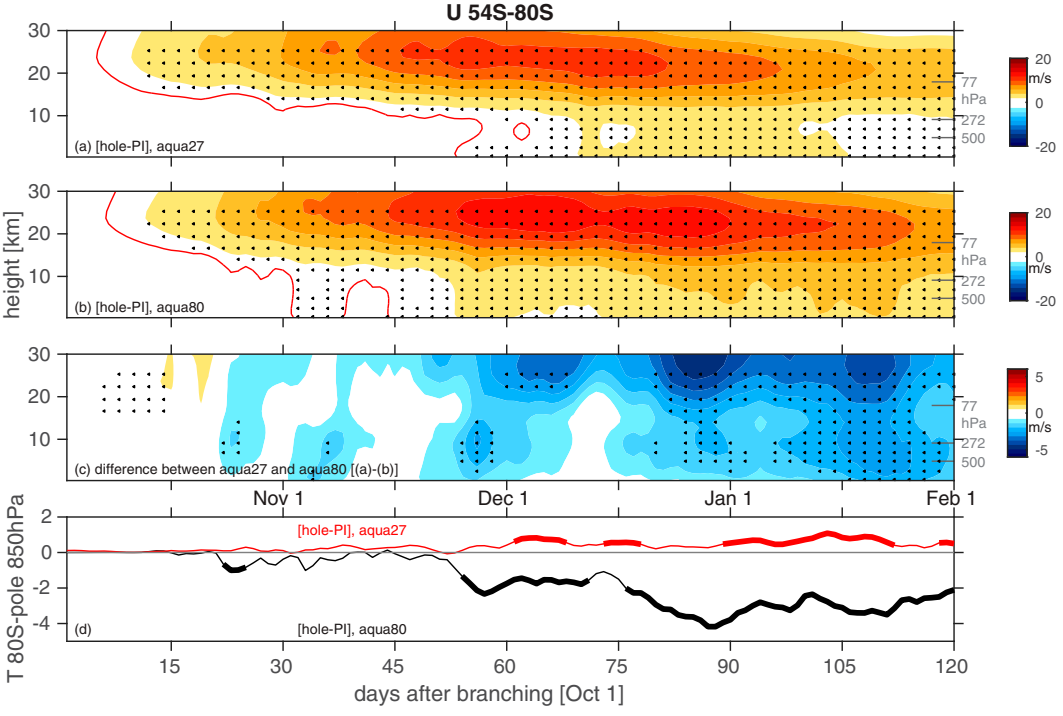

FIG. 12. Evolution of zonal wind from 54° to 80°S for the ozone hole − PI runs for an aquaplanet with Antarctic albedo equal to (a) 0.27 (AQUA27) and (b) 0.8 (AQUA80). (c) The difference between (a) and (b). The 1 m s^{-1} contour is indicated in red in (a) and (b). (d) The 80°–90°S area-weighted average temperature response (ozone hole − PI) for AQUA27 (red) and AQUA80 (black).

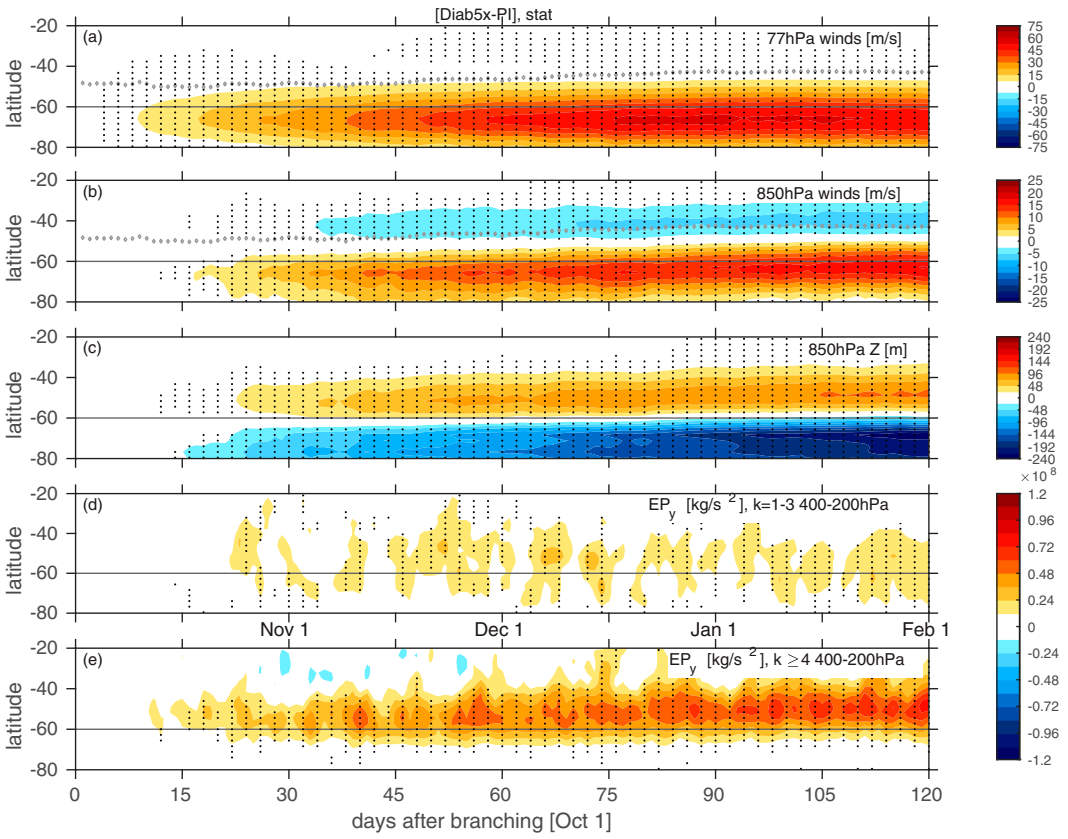

FIG. 13. As in Fig. 3, but for a diabatic heating rate of -2.5 K day^{-1} in the lower stratosphere and no ozone depletion. Note the factor-of-5 difference in the color bar for (a) and (b) and factor-of-2 difference for (c)–(e).

and free tropospheric cooling enhances the jet response. Future work should evaluate whether the stationary wave feedback or surface cooling response is crucial for the magnitude of the jet/SAM response in comprehensive models as well, and help to explain the conundrum posed by Simpson and Polvani (2016), Seviour et al. (2017), and Son et al. (2018) in which jet latitude/persistence appears to not be relevant for the magnitude of the jet and/or SAM response in many comprehensive models. Specifically, our work demonstrates that this jet latitude/persistence effect can be dwarfed by the surface cooling effect (section 6), and hence the theoretical expectation that a more persistent jet will respond more strongly to an external forcing (Chen and Plumb 2009; Garfinkel et al. 2013) may be washed out in a comprehensive model by additional processes or model biases.

Despite the negative stationary wave feedback on the magnitude of the stratospheric circulation response to ozone depletion, tropospheric planetary and synoptic waves are important for the tropospheric jet response in both AQUA80 and STAT configurations (Figs. 7 and 8). Waves 1–3 contribute roughly half of the tropospheric torque in November, although by December and January their contribution is less (Figs. 3d,e and 6d,e) in the ozone-depletion runs. In the diabatic cooling runs with an increased amplitude of the forcing to better isolate the signal (Fig. 13), synoptic waves are more important throughout; however, planetary waves still contribute.

Gravity waves also act as a negative feedback on the magnitude of the stratospheric circulation response to ozone depletion. Namely, the strengthened polar vortex allows more gravity waves to propagate into the stratosphere, and these gravity waves then break in the subpolar mid- to upper stratosphere (Fig. 10). This partial compensation between gravity waves and an externally imposed forcing is consistent with Cohen et al. (2013), Sigmond and Shepherd (2014), Scheffler and Pulido (2015), Watson and Gray (2015), and Garfinkel and Oman (2018).

The specific mechanism as to how the downward influence arises was not the main focus of this paper, although our results are of relevance to previously proposed theories. Waves 2 and 3 are crucial in the lower-stratospheric zonal momentum response [Figs. 7 and 8, consistent with Orr et al. (2012b)]. Both planetary and synoptic waves are important for the tropospheric impact, and it was not possible to distinguish whether one leads the other. This difficulty is somewhat mitigated if we enhance the signal-to-noise ratio by imposing a diabatic cooling perturbation 5 times stronger than that associated with ozone depletion (Figs. 13d,e). In response to such a strong perturbation, synoptic wavenumbers respond first, but eddy–eddy interactions still appear to be crucial for the total response

(Domeisen et al. 2013; Smith and Scott 2016). Synoptic waves are somewhat more important in summer, but in late spring the momentum forcing is more evenly split between synoptic and planetary waves for the ozone perturbations in Figs. 3d,e and 6d,e. This balance is evident both in AQUA80 and in STAT, even though stationary wave 1 is present only in STAT. The tropospheric response begins first at subpolar latitudes and only later, after synoptic eddies dominate, includes the midlatitudes. This is consistent with White et al. (2020) and White et al. (2022), who find that in the Northern Hemisphere as well, the midlatitude wind response is delayed relative to the subpolar wind response, and only occurs after synoptic eddies feedback onto the shift.

In all runs, a tropospheric response does not begin until at least 15 days after the perturbation to the stratosphere. In the diabatic cooling runs with the forcing increased by a factor of 5, there is even a weak equatorward shift in the first 10 days (although not evident in Fig. 13b using the chosen contour interval). This arises because a thermally driven cooling of the vortex will be balanced in part by downwelling over the pole and equatorward motion in the troposphere, which leads to an easterly Coriolis torque (Eliassen 1951). This opposite response is consistent with Yang et al. (2015), who find that the residual circulation is of the wrong sign to explain the poleward shift, and also with White et al. (2020), who impose a far stronger 15 K day^{-1} perturbation and find that the jet shift does not occur for at least 15 days. This effect does not explain why the observed poleward shift is not robust until December, however, as this delay is far longer than 15 days.

On the other hand, our simulations help to clarify the important factors for the onset of the response, and thereby help explain why the SAM response in observations (and in our STAT configuration) becomes robust only in summer after the ozone hole is already filling up. Namely, the tropospheric response can begin in late October if the forcing is strong (Fig. 13b) or stationary waves are absent (Fig. 6b). Even in STAT, a robust but non-SAM like response is evident in November as well; this early response is characterized by an acceleration of winds only on the subpolar flank of the jet. The net effect is that the delay of the SAM response until December in STAT is a consequence of the negative stationary wave feedback and the relative weakness of the diabatic cooling perturbation associated with ozone depletion.

The response to an identical ozone perturbation imposed in the Northern Hemisphere in STAT (STATNH) is significantly weaker than when imposed in the Southern Hemisphere (Fig. S5 in the online supplemental material). In other words, the tropospheric circulation in the Northern Hemisphere is less sensitive to a stratospheric ozone perturbation. The negative stationary wave feedback likely plays a role. Northern Hemisphere stationary waves are stronger, and hence the stratospheric circulation response to an identical ozone depletion is weaker due to an offset by enhanced wave propagation and convergence in the stratosphere. In addition, the annular mode time scale is shorter in the Northern Hemisphere (22 days vs 37 days; Fig. 9), and hence synoptic eddy feedbacks are weaker too.

In the most realistic configuration (STAT), the model simulates a response resembling that observed and simulated by comprehensive models (Figs. 1–3). Nevertheless, the model used in this work suffers from some limitations: there is no coupling of the ozone with the dynamics, the imposed ozone hole has no zonal structure, and the land surface properties over Antarctica are highly idealized including a constant albedo for all shortwave wavelengths. Despite these limitations, the results of our work have implications for seasonal forecasting and for the interpretation of results from both comprehensive and idealized models. First, interannual variability in ozone concentrations can be used to enhance seasonal forecasting (Fig. 9), consistent with Hendon et al. (2020), Jucker and Goyal (2022), and Oh et al. (2022). Second, dry and flat idealized models miss the stationary wave effect, which may lead to an exaggerated stratospheric response to a given stratospheric diabatic perturbation. Third, the Antarctic surface temperature response to ozone depletion and the climatological stationary wave magnitude helps regulate the magnitude of the jet response, and it is not clear how well models can capture the stable boundary layers common over Antarctica, the mixed-phase and ice clouds common at these latitudes, or the properties of a glaciated land surface. Further, models suffer from stationary wave biases in the Southern Hemisphere due to a double intertropical convergence zone and poorly resolved Agulhas Current Garfinkel et al. (2020a). Future work should explore whether differences in how models represent these processes can explain some of the diversity in future projections of climate change in the Southern Hemisphere (Gerber and Son 2014) and thereby help to narrow projections as ozone recovers.

Acknowledgments. Authors Garfinkel, White, and Gerber acknowledge the support of a European Research Council starting grant under the European Union Horizon 2020 research and innovation program (grant agreement 677756). Garfinkel is also supported by Israel Science Foundation Grant 1727/21. Gerber acknowledges additional support from the U.S. NSF through Grant AGS 1852727. Author Jucker acknowledges support from the Australian Research Council (ARC) Centre of Excellence for Climate Extremes (CE170100023) and ARC Grant FL 150100035. Author Son was supported by the National Research Foundation of Korea (NRF) grant funded by the South Korean government (Ministry of Science and ICT 2017R1E1A1A01074889). We thank the reviewers for their helpful comments on earlier drafts of this paper.

Data availability statement. The version of MiMA used in this study, including the modified source code, is available online (https://github.com/ianpwhite/MiMA/releases/tag/MiMA-ThermalForcing-v1.0beta; see also https://doi.org/10.5281/zenodo.4523199).

REFERENCES

Andrews, D. G., J. R. Holton, and C. B. Leovy, 1987: *Middle Atmosphere Dynamics*. Academic Press, 489 pp.

Arblaster, J. M., G. A. Meehl, and D. J. Karoly, 2011: Future climate change in the Southern Hemisphere: Competing effects

of ozone and greenhouse gases. *Geophys. Res. Lett.*, **38**, L02701, https://doi.org/10.1029/2010GL045384.

Baldwin, M. P., D. B. Stephenson, D. W. J. Thompson, T. J. Dunkerton, A. J. Charlton, and A. O'Neill, 2003: Stratospheric memory and skill of extended-range weather forecasts. *Science*, **301**, 636–640, https://doi.org/10.1126/science.1087143.

Bandoro, J., S. Solomon, A. Donohoe, D. W. Thompson, and B. D. Santer, 2014: Influences of the Antarctic ozone hole on Southern Hemispheric summer climate change. *J. Climate*, **27**, 6245–6264, https://doi.org/10.1175/JCLI-D-13-00698.1.

Banerjee, A., J. C. Fyfe, L. M. Polvani, D. Waugh, and K.-L. Chang, 2020: A pause in Southern Hemisphere circulation trends due to the Montreal protocol. *Nature*, **579**, 544–548, https://doi.org/10.1038/s41586-020-2120-4.

Barnes, E. A., and L. Polvani, 2013: Response of the midlatitude jets, and of their variability, to increased greenhouse gases in the CMIP5 models. *J. Climate*, **26**, 7117–7135, https://doi.org/10.1175/JCLI-D-12-00536.1.

Betts, A. K., 1986: A new convective adjustment scheme. Part I: Observational and theoretical basis. *Quart. J. Roy. Meteor. Soc.*, **112**, 677–691, https://doi.org/10.1002/qj.49711247307.

——, and M. J. Miller, 1986: A new convective adjustment scheme. Part II: Single column tests using GATE wave, BOMEX, ATEX and Arctic air-mass data sets. *Quart. J. Roy. Meteor. Soc.*, **112**, 693–709, https://doi.org/10.1002/qj.49711247308.

Checa-Garcia, R., 2018: CMIP6 ozone forcing dataset: Supporting information. Zenodo, https://doi.org/10.5281/zenodo.1135127.

——, M. I. Hegglin, D. Kinnison, D. A. Plummer, and K. P. Shine, 2018: Historical tropospheric and stratospheric ozone radiative forcing using the CMIP6 database. *Geophys. Res. Lett.*, **45**, 3264–3273, https://doi.org/10.1002/2017GL076770.

Chen, G., and R. A. Plumb, 2009: Quantifying the eddy feedback and the persistence of the zonal index in an idealized atmospheric model. *J. Atmos. Sci.*, **66**, 3707–3720, https://doi.org/10.1175/2009JAS3165.1.

Chiodo, G., L. M. Polvani, and M. Previdi, 2017: Large increase in incident shortwave radiation due to the ozone hole offset by high climatological albedo over Antarctica. *J. Climate*, **30**, 4883–4890, https://doi.org/10.1175/JCLI-D-16-0842.1.

Cohen, N. Y., E. P. Gerber, and O. Bühler, 2013: Compensation between resolved and unresolved wave driving in the stratosphere: Implications for downward control. *J. Atmos. Sci.*, **70**, 3780–3798, https://doi.org/10.1175/JAS-D-12-0346.1.

Domeisen, D. I., L. Sun, and G. Chen, 2013: The role of synoptic eddies in the tropospheric response to stratospheric variability. *Geophys. Res. Lett.*, **40**, 4933–4937, https://doi.org/10.1002/grl.50943.

Eliassen, A., 1951: Slow thermally or frictionally controlled meridional circulation in a circular vortex. *Astrophys. Nor.*, **5**, 19–60.

Eyring, V., and Coauthors, 2013: Long-term ozone changes and associated climate impacts in CMIP5 simulations. *J. Geophys. Res. Atmos.*, **118**, 5029–5060, https://doi.org/10.1002/jgrd.50316.

Frierson, D. M. W., I. M. Held, and P. Zurita-Gotor, 2006: A gray-radiation aquaplanet moist GCM. Part I: Static stability and eddy scale. *J. Atmos. Sci.*, **63**, 2548–2566, https://doi.org/10.1175/JAS3753.1.

——, ——, and ——, 2007: A gray-radiation aquaplanet moist GCM. Part II: Energy transports in altered climates. *J. Atmos. Sci.*, **64**, 1680–1693, https://doi.org/10.1175/JAS3913.1.

Garcia, R. R., D. E. Kinnison, and D. R. Marsh, 2012: "World avoided" simulations with the Whole Atmosphere Community Climate Model. *J. Geophys. Res.*, **117**, D23303, https://doi.org/10.1029/2012JD018430.

Garfinkel, C. I., and L. Oman, 2018: Effect of gravity waves from small islands in the Southern Ocean on the Southern Hemisphere atmospheric circulation. *J. Geophys. Res. Atmos.*, **123**, 1552–1561, https://doi.org/10.1002/2017JD027576.

——, D. W. Waugh, and E. P. Gerber, 2013: The effect of tropospheric jet latitude on coupling between the stratospheric polar vortex and the troposphere. *J. Climate*, **26**, 2077–2095, https://doi.org/10.1175/JCLI-D-12-00301.1.

——, I. White, E. P. Gerber, and M. Jucker, 2020a: The impact of SST biases in the tropical east Pacific and Agulhas Current region on atmospheric stationary waves in the Southern Hemisphere. *J. Climate*, **33**, 9351–9374, https://doi.org/10.1175/JCLI-D-20-0195.1.

——, ——, ——, and ——, 2020b: The building blocks of Northern Hemisphere wintertime stationary waves. *J. Climate*, **33**, 5611–5633, https://doi.org/10.1175/JCLI-D-19-0181.1.

Gerber, E. P., and L. M. Polvani, 2009: Stratosphere–troposphere coupling in a relatively simple AGCM: The importance of stratospheric variability. *J. Climate*, **22**, 1920–1933, https://doi.org/10.1175/2008JCLI2548.1.

——, and S.-W. Son, 2014: Quantifying the summertime response of the austral jet stream and Hadley cell to stratospheric ozone and greenhouse gases. *J. Climate*, **27**, 5538–5559, https://doi.org/10.1175/JCLI-D-13-00539.1.

——, L. M. Polvani, and D. Ancukiewicz, 2008: Annular mode time scales in the Intergovernmental Panel on Climate Change Fourth Assessment Report models. *Geophys. Res. Lett.*, **35**, L22707, https://doi.org/10.1029/2008GL035712.

Gillett, N. P., and D. W. J. Thompson, 2003: Simulation of recent Southern Hemisphere climate change. *Science*, **302**, 273–275, https://doi.org/10.1126/science.1087440.

Gonzalez, P. L., L. M. Polvani, R. Seager, and G. J. Correa, 2014: Stratospheric ozone depletion: A key driver of recent precipitation trends in south eastern South America. *Climate Dyn.*, **42**, 1775–1792, https://doi.org/10.1007/s00382-013-1777-x.

Grise, K. M., D. W. Thompson, and P. M. Forster, 2009: On the role of radiative processes in stratosphere–troposphere coupling. *J. Climate*, **22**, 4154–4161, https://doi.org/10.1175/2009JCLI2756.1.

Hendon, H. H., D. W. J. Thompson, and M. C. Wheeler, 2007: Australian rainfall and surface temperature variations associated with the Southern Hemisphere annular mode. *J. Climate*, **20**, 2452–2467, https://doi.org/10.1175/JCLI4134.1.

——, E.-P. Lim, and S. Abhik, 2020: Impact of interannual ozone variations on the downward coupling of the 2002 Southern Hemisphere stratospheric warming. *J. Geophys. Res. Atmos.*, **125**, e2020JD032952, https://doi.org/10.1029/2020JD032952.

Hitchcock, P., and I. R. Simpson, 2016: Quantifying eddy feedbacks and forcings in the tropospheric response to stratospheric sudden warmings. *J. Atmos. Sci.*, **73**, 3641–3657, https://doi.org/10.1175/JAS-D-16-0056.1.

Hurwitz, M. M., P. A. Newman, F. Li, L. D. Oman, O. Morgenstern, P. Braesicke, and J. A. Pyle, 2010: Assessment of the breakup of the Antarctic polar vortex in two new chemistry–climate models. *J. Geophys. Res.*, **115**, D07105, https://doi.org/10.1029/2009JD012788.

——, ——, and C. I. Garfinkel, 2011: The Arctic vortex in March 2011: A dynamical perspective. *Atmos. Chem. Phys.*, **11**, 11 447–11 453, https://doi.org/10.5194/acp-11-11447-2011.

Iacono, M. J., E. J. Mlawer, S. A. Clough, and J.-J. Morcrette, 2000: Impact of an improved longwave radiation model, RRTM, on the energy budget and thermodynamic properties

of the NCAR Community Climate Model, CCM3. *J. Geophys. Res.*, **105**, 14 873–14 890, https://doi.org/10.1029/2000JD900091.

Jucker, M., and E. Gerber, 2017: Untangling the annual cycle of the tropical tropopause layer with an idealized moist model. *J. Climate*, **30**, 7339–7358, https://doi.org/10.1175/JCLI-D-17-0127.1.

——, and R. Goyal, 2022: Ozone-forced southern annular mode during Antarctic stratospheric warming events. *Geophys. Res. Lett.*, **49**, e2021GL095270, https://doi.org/10.1029/2021GL095270.

Kållberg, P., P. Berrisford, B. Hoskins, A. Simmons, S. Lamy-Thépaut, and R. Hine, 2005: ERA-40 Atlas. ERA-40 Project Rep. Series 19, 103 pp.

Kang, S. M., L. M. Polvani, J. C. Fyfe, and M. Sigmond, 2011: Impact of polar ozone depletion on subtropical precipitation. *Science*, **332**, 951–954, https://doi.org/10.1126/science.1202131.

Karpechko, A. Y., A. L. A. Maycock, M. Abalos, H. Akiyoshi, J. Arblaster, C. Garfinkel, K. Rosenlof, and M. Sigmond, 2018: Stratospheric ozone changes and climate, Chapter 5. Scientific assessment of ozone depletion. Global Ozone Research and Monitoring Project Rep. 58, 416 pp.

Kidson, J. W., 1988: Interannual variations in the Southern Hemisphere circulation. *J. Climate*, **1**, 1177–1198, https://doi.org/10.1175/1520-0442(1988)001<1177:IVITSH>2.0.CO;2.

Kushner, P. J., and L. M. Polvani, 2004: Stratosphere–troposphere coupling in a relatively simple AGCM: The role of eddies. *J. Climate*, **17**, 629–639, https://doi.org/10.1175/1520-0442(2004)017<0629:SCIARS>2.0.CO;2.

Lawrence, Z. D., J. Perlwitz, A. H. Butler, G. L. Manney, P. A. Newman, S. H. Lee, and E. R. Nash, 2020: The remarkably strong Arctic stratospheric polar vortex of winter 2020: Links to record-breaking Arctic Oscillation and ozone loss. *J. Geophys. Res. Atmos.*, **125**, e2020JD033271, https://doi.org/10.1029/2020JD033271.

Li, F., P. A. Newman, and R. S. Stolarski, 2010: Relationships between the Brewer-Dobson circulation and the southern annular mode during austral summer in coupled chemistry–climate model simulations. *J. Geophys. Res.*, **115**, D15106, https://doi.org/10.1029/2009JD012876.

Manney, G. L., and Coauthors, 2011: Unprecedented Arctic ozone loss in 2011. *Nature*, **478**, 469–475, https://doi.org/10.1038/nature10556.

Manzini, E., B. Steil, C. Brühl, M. A. Giorgetta, and K. Krüger, 2003: A new interactive chemistry–climate model: 2. Sensitivity of the middle atmosphere to ozone depletion and increase in greenhouse gases and implications for recent stratospheric cooling. *J. Geophys. Res.*, **108**, 4429, https://doi.org/10.1029/2002JD002977.

McLandress, C., A. I. Jonsson, D. A. Plummer, M. C. Reader, J. F. Scinocca, and T. G. Shepherd, 2010: Separating the dynamical effects of climate change and ozone depletion. Part I: Southern Hemisphere stratosphere. *J. Climate*, **23**, 5002–5020, https://doi.org/10.1175/2010JCLI3586.1.

——, T. G. Shepherd, J. F. Scinocca, D. A. Plummer, M. Sigmond, A. I. Jonsson, and M. C. Reader, 2011: Separating the dynamical effects of climate change and ozone depletion. Part II: Southern Hemisphere troposphere. *J. Climate*, **24**, 1850–1868, https://doi.org/10.1175/2010JCLI3958.1.

Merlis, T. M., T. Schneider, S. Bordoni, and I. Eisenman, 2013: Hadley circulation response to orbital precession. Part II: Subtropical continent. *J. Climate*, **26**, 754–771, https://doi.org/10.1175/JCLI-D-12-00149.1.

Mlawer, E. J., S. J. Taubman, P. D. Brown, M. J. Iacono, and S. A. Clough, 1997: Radiative transfer for inhomogeneous atmospheres: RRTM, a validated correlated-*k* model for the longwave. *J. Geophys. Res.*, **102**, 16 663–16 682, https://doi.org/10.1029/97JD00237.

Neely, R., D. Marsh, K. Smith, S. Davis, and L. Polvani, 2014: Biases in Southern Hemisphere climate trends induced by coarsely specifying the temporal resolution of stratospheric ozone. *Geophys. Res. Lett.*, **41**, 8602–8610, https://doi.org/10.1002/2014GL061627.

Newman, P. A., and Coauthors, 2009: What would have happened to the ozone layer if chlorofluorocarbons (CFCs) had not been regulated? *Atmos. Chem. Phys.*, **9**, 2113–2128, https://doi.org/10.5194/acp-9-2113-2009.

Ogawa, F., N.-E. Omrani, K. Nishii, H. Nakamura, and N. Keenlyside, 2015: Ozone-induced climate change propped up by the Southern Hemisphere oceanic front. *Geophys. Res. Lett.*, **42**, 10 056–10 063, https://doi.org/10.1002/2015GL066538.

Oh, J., S.-W. Son, J. Choi, E.-P. Lim, C. Garfinkel, H. Hendon, Y. Kim, and H.-S. Kang, 2022: Impact of stratospheric ozone on the subseasonal prediction in the Southern Hemisphere spring. *Prog. Earth Planet. Sci.*, **9**, 25, https://doi.org/10.1186/s40645-022-00485-4.

Orr, A., T. J. Bracegirdle, J. S. Hosking, W. Feng, H. K. Roscoe, and J. D. Haigh, 2012a: Strong dynamical modulation of the cooling of the polar stratosphere associated with the Antarctic ozone hole. *J. Climate*, **26**, 662–668, https://doi.org/10.1175/JCLI-D-12-00480.1.

——, ——, ——, T. Jung, J. D. Haigh, T. Phillips, and W. Feng, 2012b: Possible dynamical mechanisms for Southern Hemisphere climate change due to the ozone hole. *J. Atmos. Sci.*, **69**, 2917–2932, https://doi.org/10.1175/JAS-D-11-0210.1.

Polvani, L. M., M. Previdi, and C. Deser, 2011a: Large cancellation, due to ozone recovery, of future Southern Hemisphere atmospheric circulation trends. *Geophys. Res. Lett.*, **38**, L04707, https://doi.org/10.1029/2011GL046712.

——, D. W. Waugh, G. J. P. Correa, and S.-W. Son, 2011b: Stratospheric ozone depletion: The main driver of twentieth-century atmospheric circulation changes in the Southern Hemisphere. *J. Climate*, **24**, 795–812, https://doi.org/10.1175/2010JCLI3772.1.

Previdi, M., and L. M. Polvani, 2014: Climate system response to stratospheric ozone depletion and recovery. *Quart. J. Roy. Meteor. Soc.*, **140**, 2401–2419, https://doi.org/10.1002/qj.2330.

Randel, W. J., and Coauthors, 2009: An update of observed stratospheric temperature trends. *J. Geophys. Res.*, **114**, D02107, https://doi.org/10.1029/2008JD010421.

Rao, J., and C. I. Garfinkel, 2020: Arctic ozone loss in March 2020 and its seasonal prediction in CFSv2: A comparative study with the 1997 and 2011 cases. *J. Geophys. Res. Atmos.*, **125**, e2020JD033524, https://doi.org/10.1029/2020JD033524.

——, and ——, 2021: CMIP5/6 models project little change in the statistical characteristics of sudden stratospheric warmings in the 21st century. *Environ. Res. Lett.*, **16**, 034024, https://doi.org/10.1088/1748-9326/abd4fe.

Scheffler, G., and M. Pulido, 2015: Compensation between resolved and unresolved wave drag in the stratospheric final warmings of the Southern Hemisphere. *J. Atmos. Sci.*, **72**, 4393–4411, https://doi.org/10.1175/JAS-D-14-0270.1.

Seviour, W. J. M., D. W. Waugh, L. M. Polvani, G. J. P. Correa, and C. I. Garfinkel, 2017: Robustness of the simulated tropospheric response to ozone depletion. *J. Climate*, **30**, 2577–2585, https://doi.org/10.1175/JCLI-D-16-0817.1.

Sheshadri, A., and R. A. Plumb, 2016: Sensitivity of the surface responses of an idealized AGCM to the timing of imposed

ozone depletion-like polar stratospheric cooling. *Geophys. Res. Lett.*, **43**, 2330–2336., https://doi.org/10.1002/2016GL067964.

Sigmond, M., and T. G. Shepherd, 2014: Compensation between resolved wave driving and parameterized orographic gravity wave driving of the Brewer–Dobson circulation and its response to climate change. *J. Climate*, **27**, 5601–5610, https://doi.org/10.1175/JCLI-D-13-00644.1.

Simpson, I. R., and L. M. Polvani, 2016: Revisiting the relationship between jet position, forced response, and annular mode variability in the southern midlatitudes. *Geophys. Res. Lett.*, **43**, 2896–2903, https://doi.org/10.1002/2016GL067989.

Smith, K. L., and R. K. Scott, 2016: The role of planetary waves in the tropospheric jet response to stratospheric cooling. *Geophys. Res. Lett.*, **43**, 2904–2911, https://doi.org/10.1002/2016GL067849.

Solomon, S., R. R. Garcia, F. S. Rowland, and D. J. Wuebbles, 1986: On the depletion of Antarctic ozone. *Nature*, **321**, 755–758, https://doi.org/10.1038/321755a0.

——, R. W. Portmann, T. Sasaki, D. J. Hofmann, and D. W. Thompson, 2005: Four decades of ozonesonde measurements over Antarctica. *J. Geophys. Res.*, **110**, D21311, https://doi.org/10.1029/2005JD005917.

Son, S.-W., and Coauthors, 2008: The impact of stratospheric ozone recovery on the Southern Hemisphere westerly jet. *Science*, **320**, 1486–1489, https://doi.org/10.1126/science.1155939.

——, and Coauthors, 2010: Impact of stratospheric ozone on Southern Hemisphere circulation change: A multimodel assessment. *J. Geophys. Res.*, **115**, D00M07, https://doi.org/10.1029/2010JD014271.

——, A. Purich, H. H. Hendon, B.-M. Kim, and L. M. Polvani, 2013: Improved seasonal forecast using ozone hole variability? *Geophys. Res. Lett.*, **40**, 6231–6235, https://doi.org/10.1002/2013GL057731.

——, and Coauthors, 2018: Tropospheric jet response to Antarctic ozone depletion: An update with Chemistry–Climate Model Initiative (CCMI) models. *Environ. Res. Lett.*, **13**, 054024, https://doi.org/10.1088/1748-9326/aabf21.

Stolarski, R. S., A. R. Douglass, M. Gupta, P. A. Newman, S. Pawson, M. R. Schoeberl, and J. E. Nielsen, 2006: An ozone increase in the Antarctic summer stratosphere: A dynamical response to the ozone hole. *Geophys. Res. Lett.*, **33**, L21805, https://doi.org/10.1029/2006GL026820.

Sun, L., G. Chen, and W. A. Robinson, 2014: The role of stratospheric polar vortex breakdown in Southern Hemisphere climate trends. *J. Atmos. Sci.*, **71**, 2335–2353, https://doi.org/10.1175/JAS-D-13-0290.1.

Thompson, D. W. J., and J. M. Wallace, 2000: Annular modes in the extratropical circulation. Part I: Month-to-month variability. *J. Climate*, **13**, 1000–1016, https://doi.org/10.1175/1520-0442(2000)013<1000:AMITEC>2.0.CO;2.

——, S. Solomon, P. J. Kushner, M. H. England, K. M. Grise, and D. J. Karoly, 2011: Signatures of the Antarctic ozone hole in Southern Hemisphere surface climate change. *Nat. Geosci.*, **4**, 741–749, https://doi.org/10.1038/ngeo1296.

Trenberth, K. E., and D. P. Stepaniak, 2002: A pathological problem with NCEP reanalysis in the stratosphere. *J. Climate*, **15**, 690–695, https://doi.org/10.1175/1520-0442(2002)015<0690:APPWNR>2.0.CO;2.

Ummenhofer, C. C., A. S. Gupta, and M. H. England, 2009: Causes of late twentieth-century trends in New Zealand precipitation. *J. Climate*, **22**, 3–19, https://doi.org/10.1175/2008JCLI2323.1.

Watson, P. A. G., and L. J. Gray, 2015: The stratospheric wintertime response to applied extratropical torques and its relationship with the annular mode. *Climate Dyn.*, **44**, 2513–2537, https://doi.org/10.1007/s00382-014-2359-2.

Waugh, D. W., C. Garfinkel, and L. M. Polvani, 2015: Drivers of the recent tropical expansion in the Southern Hemisphere: Changing SSTS or ozone depletion? *J. Climate*, **28**, 6581–6586, https://doi.org/10.1175/JCLI-D-15-0138.1.

Weber, M., M. Coldewey-Egbers, V. E. Fioletov, S. M. Frith, J. D. Wild, J. P. Burrows, C. S. Long, and D. Loyola, 2018: Total ozone trends from 1979 to 2016 derived from five merged observational datasets—The emergence into ozone recovery. *Atmos. Chem. Phys.*, **18**, 2097–2117, https://doi.org/10.5194/acp-18-2097-2018.

White, I. P., C. I. Garfinkel, E. P. Gerber, M. Jucker, P. Hitchcock, and J. Rao, 2020: The generic nature of the tropospheric response to sudden stratospheric warmings. *J. Climate*, **33**, 5589–5610, https://doi.org/10.1175/JCLI-D-19-0697.1.

——, ——, and P. Hitchcock, 2022: On the tropospheric response to stratospheric momentum torques. *J. Climate*, 79, 2041–2058, https://doi.org/10.1175/JAS-D-21-0237.1.

World Meteorological Organization, 2011: Scientific assessment of ozone depletion: 2010. Global Ozone Research and Monitoring Project Rep. 52, 516 pp.

——, 2014: Scientific assessment of ozone depletion: 2014. Global Ozone Research and Monitoring Project Rep. 55, 416 pp.

Yang, H., L. Sun, and G. Chen, 2015: Separating the mechanisms of transient responses to stratospheric ozone depletion–like cooling in an idealized atmospheric model. *J. Atmos. Sci.*, **72**, 763–773, https://doi.org/10.1175/JAS-D-13-0353.1.

Yang, J., Q. Bao, D. Ji, D. Gong, R. Mao, Z. Zhang, and S.-J. Kim, 2014: Simulation and causes of eastern Antarctica surface cooling related to ozone depletion during austral summer in FGOALS-s2. *Adv. Atmos. Sci.*, **31**, 1147–1156, https://doi.org/10.1007/s00376-014-3144-1.

Young, P., S. M. Davis, B. Hassler, S. Solomon, and K. Rosenlof, 2014: Modeling the climate impact of Southern Hemisphere ozone depletion: The importance of the ozone data set. *Geophys. Res. Lett.*, **41**, 9033–9039, https://doi.org/10.1002/2014GL061738.